nature geoscience

ARTICLES

https://doi.org/10.1038/s41561-018-0210-9

Concomitant variability in high-latitude aerosols, water isotopes and the hydrologic cycle

Bradley R. Markle[1,2*], Eric J. Steig[1], Gerard H. Roe[1], Gisela Winckler[3] and Joseph R. McConnell[4]

The interpretation of ice-core records rests on understanding the processes affecting trace constituents of the atmosphere that are preserved in ice. Stable-isotope ratios of ice are widely used as a palaeothermometer, an interpretation backed by well-established theory. In contrast, the interpretation of aerosols such as mineral dust and sea salts has remained a topic of debate. Here, we demonstrate that both the fractionation of water isotopes and the scavenging of aerosols are fundamentally driven by the same process, the condensation of water from the atmosphere. Water isotope ratios and aerosol concentrations in ice cores are remarkably coherent on all timescales longer than a few centuries. This shared low-frequency variability is dominated by the essential physics of the hydrologic cycle, which also accounts for the difference in variability between marine- and terrestrial-sourced aerosols in ice cores, as well as the global spatial pattern of aerosol changes recorded in both marine sediments and ice. These results have implications for past changes in radiative forcing and other fundamental aspects of climate, such as polar amplification, which are imprinted on the relationships between these proxy records.

Stable-isotope ratios of oxygen and hydrogen in polar ice reflect the integrated evaporation and condensation history of moisture in the atmosphere and are a commonly used proxy for condensation temperature[1–3]. Aerosols, including dust and sea-salt, are transported from lower-latitude sources to Antarctica and preserved as impurities in the ice[4–6]. Ice-core records of dust and sea-salt show orders-of-magnitude variability between climate states[7–9]. While the origin of this variability is debated, there is a long-standing view that changes in aerosol source emissions are the primary driver[7–11].

Numerous environmental conditions influence dust source emission strength, including wind speed[7], gustiness[12], aridity, continental-shelf area, soil moisture, land cover, vegetation[9,13,14] and glacial activity[15,16]. South America is the dominant source area for dust reaching Antarctica[17,18]. The environmental conditions that influence sea-salt emissions are less clear[8,19]. Sea spray is a source of aerosolized sea salts that depends on wind speed and open-ocean area[7]. Frost flowers on sea ice are also a source of sea-salt aerosols[20], although evidence that this source makes a substantial contribution to Antarctic ice impurities is mixed[9,21]. While sea-salt emissions are often linked to sea ice area, even the sign of this relationship is debated[8,19].

A striking covariation is consistently observed between water isotope ratios and impurities in Antarctic ice cores[11,22,23] (Fig. 1). It has been claimed that this correspondence reflects broad coupling of the climate system[7,11,24], linking disparate environmental features such as Antarctic temperature and the variety of factors that influence South American dust emission and Southern Ocean sea-salt sources.

Proxy records from the West Antarctic Ice Sheet Divide ice core (WDC)[22,23,25], the highest-resolution Antarctic records to span the last deglaciation, reveal the nature of the relationship between Antarctic water isotopes and aerosols in unprecedented detail. The $\delta^{18}O$ variability in WDC is highly anticorrelated with the logarithm of the concentration of non-sea-salt calcium (nssCa, directly related to the dust impurity) and sea-salt sodium (ssNa). The complete WDC impurity records from 6 ka to 67 ka (ka is thousand years ago) are presented here. The exponential relationship to water isotope variability explains more than 75% of the variance in the dust record (coefficient of correlation $r = -0.87$ for nssCa) and 65% of the variance in the sea-salt record ($r = -0.83$ for ssNa). This relationship consistently describes the records at multi-centennial, millennial and orbital timescales (Supplementary Information).

The evident simplicity of the relationship between water isotopes and aerosols stands in contrast to the ambiguity in the prevailing paradigm. It would be surprising if the processes driving dust and sea-salt emission were to covary so consistently, both with one another and with the independent processes driving water isotope distillation. Further, the processes that could lead to 10-fold to 100-fold changes in either dust or sea-salt emissions remain unknown. Comprehensive climate models that include many mechanisms for aerosol emission changes do not reproduce such large variability in aerosol source strength between climate states[14,16,18,26,27]. Finally, changes in dust sources cannot explain why mid-latitude sediment-core records of dust deposition nearer to the dust sources show order-of-magnitude less variability than those from Antarctica[18,24,28–30].

A simple water isotope and aerosol model

Parsimony suggests that a single mechanism unites the water isotope and aerosol records. The clear exponential relationships shown in Fig. 1c call for exponential physics. We propose that the correlation between these proxies may be readily explained if their variability on climatological timescales is primarily driven by the condensation and precipitation of water.

High-latitude water isotope ratios are widely understood to record the progressive distillation of water transported toward the poles[1–3]. Central to this process is the exponential dependence of the atmosphere's saturated vapour pressure on temperature, the Clausius–Clapeyron relation, which drives the condensation and precipitation of moisture.

[1]Department of Earth and Space Sciences, University of Washington, Seattle, WA, USA. [2]Earth Research Institute, University of California Santa Barbara, Santa Barbara, CA, USA. [3]Lamont-Doherty Earth Observatory of Columbia University, Palisades, NY, USA. [4]Desert Research Institute, Reno, NV, USA. *e-mail: marklebr@uw.edu

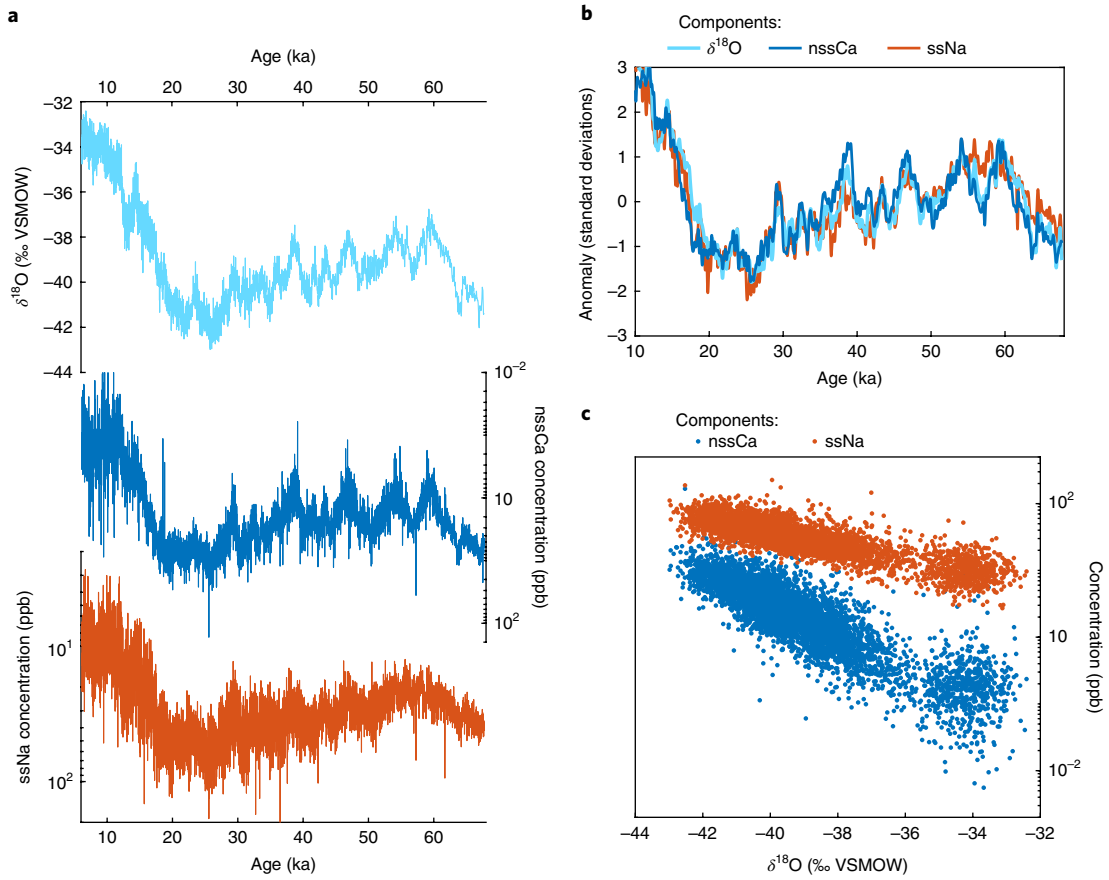

Fig. 1 | Data from the WAIS Divide ice core. a, WDC δ^{18}O (top, light blue), nssCa (middle, dark blue) and ssNa (bottom, red). Note the inverted axes of aerosols. **b**, Low-pass filtered records (δ^{18}O and the log of the aerosol concentrations, inverted), presented as *z*-score anomalies (difference from the record mean, divided by the standard deviation). High-frequency variability (>1/300 yr^{-1}) removed with a low-pass Butterworth filter. **c**, WDC δ^{18}O plotted against nssCa (blue) and ssNa (red). Time series are from 6 ka to 68 ka; aerosol data are available only from below the brittle zone of the core. Stable-isotope ratios of oxygen in water are reported as delta values: $\delta^{18}O = (R^{18}_{sample} - R^{18}_{VSMOW}) / R^{18}_{VSMOW}$, where R^{18}_{sample} is the number ratio of heavy to light oxygen isotopes in a sample, $R^{18} = \frac{^{18}O}{^{16}O}$, and R^{18}_{VSMOW} is the number ratio in Vienna Standard Mean Ocean Water (VSMOW). ppb, parts per 10^9.

Aerosols are removed from the atmosphere by wet and dry deposition[6,31]. Globally, wet deposition is the dominant mechanism of aerosol removal[32]; aerosols act as condensation nuclei and are scavenged by precipitation[6,27]. Dry deposition involves gravitational settling and turbulent interaction with the surface[6]. The amount of aerosol removed from the atmosphere by either wet or dry deposition depends on the concentration[16]. This leads to exponential decay of aerosol concentration during transport from the source (Methods).

The idea that the processes of condensation and rainout may drive aerosol variability on long timescales is not new[31], although its relevance has been debated[6,8,11,14,19]. Because water isotope ratios are driven by the same fundamental process, the relationships between these proxies can provide novel constraints on the role of the hydrologic cycle. Here, we investigate the influence of progressive rainout on both aerosols and water isotope ratios, and determine what relationships between them should be expected due to this process.

We construct a simple model of water isotope distillation and aerosol rainout (Methods). We consider a latitudinal temperature gradient from the mid-latitudes to the pole, and the transport of moisture and aerosols down this gradient. Moisture is removed from the atmosphere due to the condensation implied by the temperature dependence of the Clausius–Clapeyron relation. Water isotopes are distilled from characteristic source regions[25,33] to the deposition site following well-established fractionation equations[1,2,34,35]. Aerosols are transported from source regions[18,36] and removed from the atmosphere by rainout, accounting for characteristic scavenging efficiencies and the latitudinal distribution of precipitation (see Methods and Supplementary Information). Due to rainout, the natural logarithm of the aerosol concentration along the transport path is inversely proportional to the integrated precipitation along the path.

Results

We first consider the modern Southern Hemisphere temperature gradient[37] (Fig. 2a, red line) and the associated latitudinal profile in the saturated mixing ratio (Fig. 2b), which dictates condensation during transport. This moisture distillation leads to the well-known poleward depletion of water isotope ratios in precipitation (Fig. 2c). We calculate the change in aerosol concentration of nssCa and ssNa owing to the integrated precipitation (Fig. 2d). Aerosol concentrations decay exponentially by several orders of magnitude between source and final deposition in Antarctica, in agreement both with observations of modern atmospheric aerosol burdens and with calculations from comprehensive models[27].

We next examine the effect of cooling temperature uniformly at all latitudes (Fig. 2, yellow lines), as well as cooling to a temperature gradient representative of the Last Glacial Maximum (LGM; blue lines). The LGM was ~10 °C colder at the WDC site[38], while tropical temperatures were ~3–4 °C colder[39,40]. Initial aerosol source concentrations are assumed to be fixed.

Colder temperature profiles deplete the δ^{18}O of precipitation at high latitudes (Fig. 2c), reflecting increases in moisture distillation. The same hydrologic changes exponentially increase the aerosol

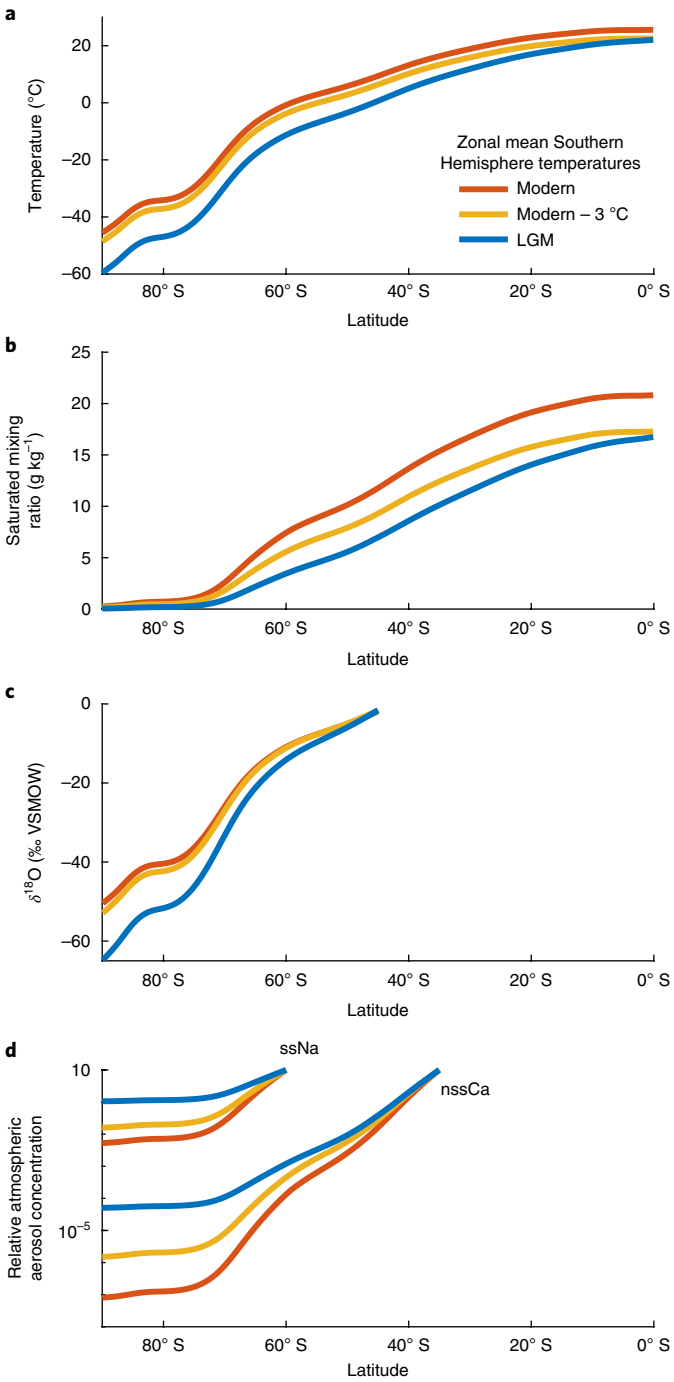

Fig. 2 | Simple model results for zonal mean temperature gradients. **a**, Zonal mean Southern Hemisphere temperature: modern (red), cooled 3 °C (yellow) and LGM-like (blue). The following panels show modelled variables for each of these mean states. **b**, Saturated mixing ratio of the atmosphere. **c**, The δ^{18}O of precipitation along the path from the evaporation source (45° S) toward the pole. **d**, Atmospheric aerosol concentration along the path from the initial source for nssCa (35° S) and ssNa (60° S). Initial aerosol concentrations are fixed between states, and we assume no dry deposition for simplicity. We use scavenging efficiencies for nssCa and ssNa based on central estimates from a compilation of studies (Supplementary Table 1).

concentration reaching higher latitudes (Fig. 2d). In a colder climate, the atmosphere holds less moisture, has a reduced gradient in the saturated mixing ratio and thus has less integrated precipitation between the source and deposition sites. Exponentially more aerosols are able to reach the polar regions in cold climates simply because exponentially fewer are removed along the way, independent of any changes in the source emission.

We integrate our model through a spectrum of temperature profiles, from modern to LGM-like, to reproduce the range of water isotope variability observed in the WDC record. We calculate the associated changes in aerosol concentration owing to changes in wet removal and calculate the amplification of concentrations between climate states. The amplification factor of an aerosol concentration is the change in concentration with respect to a reference period (the LGM in this comparison). We compare the modelled relationships of high-latitude water isotopes to dust and sea-salt amplification with those same relationships observed in the ice-core record (Fig. 3).

We assess the model's sensitivity to source emission strength, source latitude, the mass-scavenging ratio and polar amplification. Our conclusions are robust to both uncertainty and plausible variability in all of these parameters (Fig. 3b–d and Supplementary Information).

Discussion

Our results show that temperature-driven changes in rainout lead to orders-of-magnitude changes in Antarctic aerosol concentrations, in excellent agreement with ice-core records. No changes in source emission or transport time are required. The condensation and rainout process naturally leads to the observed negative-exponential relationship between aerosol concentrations and water isotope ratios. This relationship does not arise from coupling of disparate parts of the climate system for which aerosols and water isotopes are independent proxies. Rather, the condensation history of the atmosphere drives concomitant variability in both water isotopes and aerosols. Specifically, aerosol concentrations vary inversely and exponentially with the total amount of moisture removed from the atmosphere between mid- and high latitudes, which increases with mean temperature. Water isotope ratios reflect total atmospheric distillation, the fraction of mid-latitude moisture that reaches the high latitudes, which also increases with global temperature. This is the ultimate source of the negative-exponential relationship, which accounts for the overwhelming majority of the variance (>80%) in the records, particularly at multi-centennial and longer timescales. Explanations of long-term high-latitude aerosol variability that rely on source emission strength alone are not inherently exponential.

Our model accounts for important features of the proxy records that have either remained unexplained or required multiple separate explanations. For example, marine aerosols (such as ssNa) show smaller glacial–interglacial change than terrestrial aerosols such as dust and nssCa, and thus a shallower slope in the relationship to water isotopes (Fig. 3). Our calculations show that this is a result of the different mean source latitudes for ssNa and nssCa. While the scavenging efficiencies of the two aerosols are similar, the Southern Ocean source of marine aerosols is closer to Antarctica than the continental source of dust. Marine aerosols thus experience less of the rainout pathway and therefore less variability due to changes in integrated rainout.

The relationship between source latitude and integrated rainout explains why South America, rather than other Southern Hemisphere continents, is the dominant dust source for Antarctica[17,18]. Aerosols from more northerly sources must transit more of the meridional temperature gradient and rainout pathway and are thus exponentially less likely to reach Antarctica on average (Supplementary Information).

Additional factors certainly contribute to variability in the aerosol records. At timescales shorter than multi-centennial, the negative-exponential relationship between water isotopes and aerosols is overwhelmed by other high-frequency variability (Supplementary Information), accounting for the scatter around the modelled

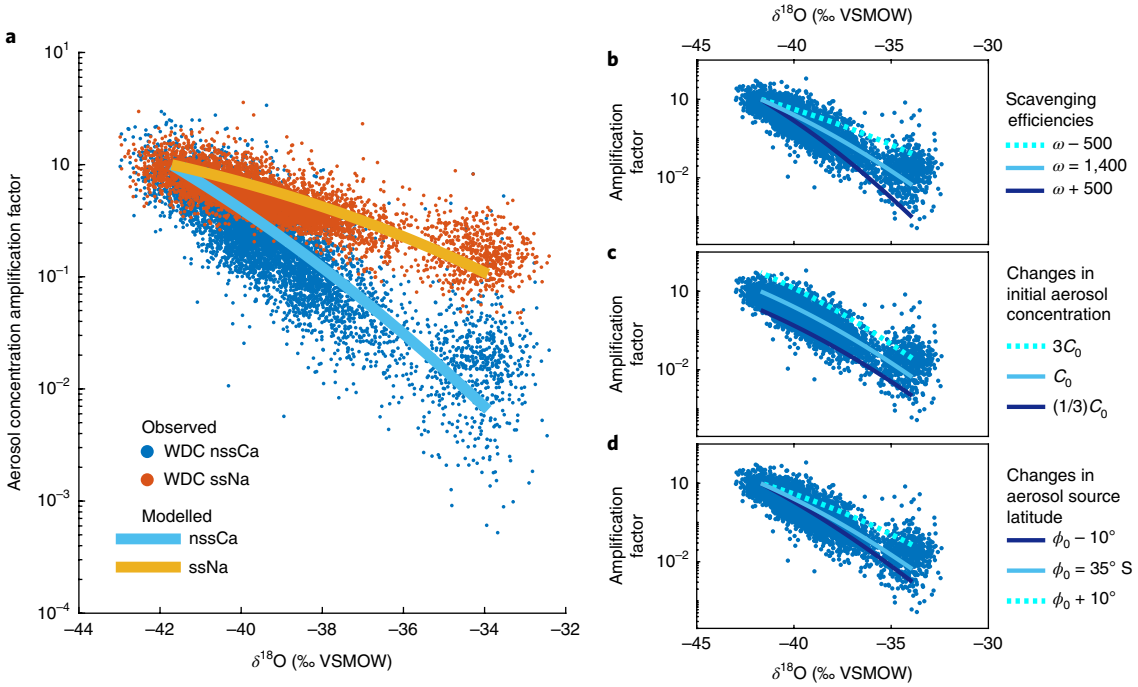

Fig. 3 | Comparison of observations and model. a, Observed relationship between WDC δ^{18}O and nssCa (blue dots) and ssNa (red dots), compared with the modelled relationships (light blue and yellow lines, respectively). Aerosol amplification factors are the concentration divided by the mean concentration during the LGM (20–25 ka). **b**–**d**, Sensitivity of model relationship between δ^{18}O and nssCa (lines) to model parameters. WDC observations are shown as blue dots. Modelled ssNa sensitivity shows similar behaviour (not shown). Sensitivity to mass-scavenging efficiency parameter, $\omega = 1,400 \pm 500$ (ω is in units of $\frac{\text{g aerosol}}{\text{g precipitation}} \div \frac{\text{g aerosol}}{\text{g air}}$) (**b**). Sensitivity to an instantaneous threefold increase or decrease in initial aerosol source concentration, C_0 (**c**). Sensitivity to a ±10° change in aerosol source latitude, ϕ_0, of 35° S (**d**).

relationship (Fig. 3). This scatter has a log-normal distribution, which is expected if the variability is modulated by an underlying, inherently exponential process such as rainout. The longer the rainout pathway, the more the exponential physics dominates the signal over the noise. This is why terrestrial aerosols, which have a longer pathway than marine aerosols, show a larger signal-to-noise ratio (Fig. 1).

The importance of the rainout process is not limited to Antarctica. We compare δ^{18}O and nssCa from WDC with an equivalent record from the opposite pole: the Greenland Ice-core Project (GRIP) ice-core record[41] (Fig. 4a). The GRIP and WDC sites have similar modern temperature, accumulation and δ^{18}O values[22], as well as similar glacial–interglacial changes in δ^{18}O. The amplification of GRIP nssCa since the LGM is nearly identical to that at the WDC site. Both records show the same negative-exponential relationship between nssCa and δ^{18}O, with similar scatter. These remarkable similarities arise even though the time series themselves are distinct between the hemispheres, with different patterns of millennial variability and timings of deglaciation. Greenland and Antarctica have separate dust sources with different sensitivities to source region conditions such as windiness, aridity, vegetation and continental-shelf expansion[14]. It is prohibitively unlikely that this wide range of variables would consistently combine to result in dust variability at each pole that has an identical exponential relationship to local δ^{18}O. In contrast, the observed δ^{18}O variability requires a change in atmospheric condensation that our model predicts must have driven the observed orders-of-magnitude variability in dust aerosols reaching those sites, regardless of changes in dust emission.

The rainout model predicts that the difference in aerosol concentrations between climate states should increase exponentially toward the pole from the aerosol source (Fig. 2). We compare Antarctic dust records (WDC nssCa, as well as nssCa and dust flux from the European Project for Ice Coring in Antarctica (EPICA) ice core from Dome Concordia (EDC))[42,43] with two marine sediment-core dust flux records (corrected for sediment redistribution)[30], from the South Atlantic and downwind of South American dust sources, and with a suite of South Pacific marine sediment-core records[24] from north of the WDC site (Fig. 4b). All of the records show more dust during the LGM, but while the ice-core records show 20-fold to 100-fold amplification, the marine records are amplified by factors of just 3 to 6.

We examine the global pattern of LGM dust amplification revealed by the above records and two compilations of dust flux changes, one from marine sediment cores that have been corrected for sediment redistribution[44], and another of dust flux changes from additional sediment-core and ice-core records[18]. The global spatial pattern shows unambiguous exponential poleward amplification of dust changes in the mid- and high latitudes, correctly predicted by our rainout model (Fig. 4c,d). This global spatial pattern is inconsistent with source region dust emissions being the dominant source of glacial–interglacial variability, which would lead to equal amplification at all latitudes. In fact, as shown in Fig. 4d, we should expect a poleward increase in dust due to reduced rainout, even if source emissions decreased during the LGM.

Aerosol emissions change with global climate. However, the low-frequency variability in ice-core records is not necessarily evidence of these changes. Lower-latitude records may provide more insight into dust source dynamics and are consistent with 0.5-fold to 4-fold changes, with a central estimate of a 2-fold to 3-fold source emission increase during the LGM. They show no evidence for the 10-fold to 100-fold changes seen in ice cores.

While the rainout mechanism correctly predicts the negative-exponential relationship between aerosols and water isotopes, we note that the slope of this relationship in WDC is reduced at the most enriched δ^{18}O values (the Holocene). This pattern, a change in the negative-exponential slope during warmer climates, is also

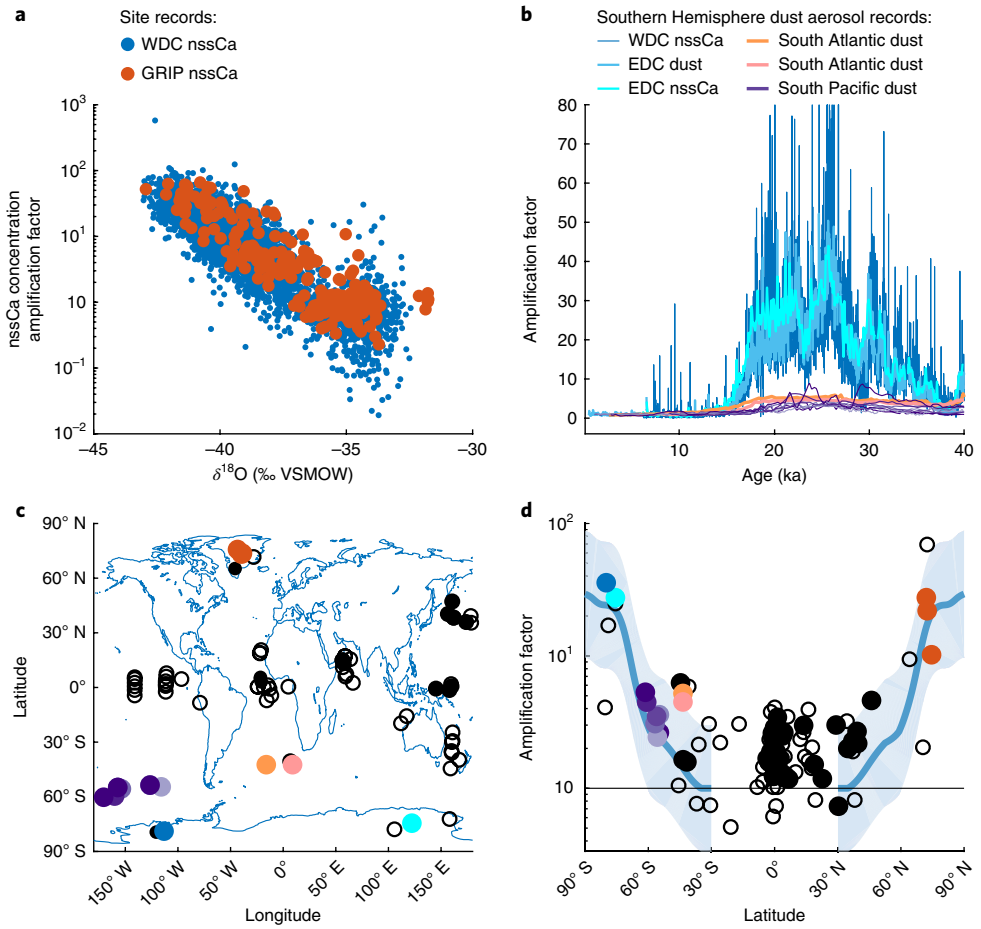

Fig. 4 | Global pattern of dust changes. a, δ^{18}O and nssCa amplification (with respect to early Holocene 6–10 ka) from WDC (blue) and GRIP (red). **b**, Time series of Southern Hemisphere dust aerosol amplification records: WDC nssCa (blue); EDC nssCa (light blue); EDC dust (cyan); two marine dust flux records, corrected for sediment redistribution, from the South Atlantic[30] (orange and pink); and several South Pacific records[24] (purple). **c**, Locations of records in **a** and **b** (coloured consistently), as well as nssCa records from the North Greenland Ice-core Project and the Greenland Ice Sheet Project 2 (red)[45], and two global compilations of dust flux changes, one from marine sediment cores corrected for sediment redistribution[44] (black filled circles) and a second from additional sediment and ice cores[18] (open circles). **d**, Dust amplification against latitude for all records shown in **c**. The expected global spatial pattern of dust aerosol amplification from the simple model, given rainout poleward of 35° N and 35° S, and no change in source emission (dark blue line). Shading shows the influence of 1/3-fold to 3-fold change in source emission.

observed in Greenland[45] and in East Antarctic dust records across multiple glacial cycles[11,42] (Supplementary Fig. 8). Sea-salt records also show curvature in the negative-exponential relationship, but of opposite sign to that in the dust[42] (Supplementary Information).

The rainout model does not predict a strictly linear relationship between the log of aerosol concentrations and the water isotope ratios. Due to its influence on integrated condensation, changes in the Equator-to-pole temperature gradient (such as polar amplification) can result in curvature of the negative-exponential relationship. The shape of this curvature depends on both the source latitude of each aerosol and the ice-core site latitude. However, the essential negative-exponential relationship is robust to uncertainty in the magnitude of polar amplification. Moreover, physically plausible patterns of polar amplification result in the observed sign of curvature in the relationships of both sea salts and dust (Supplementary Information). A change in the scavenging efficiency with climate would also influence these slopes.

Our results suggest that the condensation process dominates high-latitude aerosol variability, but this is not the only source of variability. Changes in aerosol source strength and source latitude, acting concurrently with rainout, will also change the slope of the negative-exponential relationship. The flattening of the relationship in WDC during the Holocene is consistent with a modest increase in source emission and/or a poleward shift of source latitude during the Holocene (Fig. 3). Likewise, a relatively small increase in interglacial dust source strength and/or a modest poleward shift in interglacial source latitude, superimposed on the dominant rainout process, would consistently explain the dust relationship observed in East Antarctica across the last eight glacial cycles (Supplementary Fig. 9).

By accounting for the influence of the rainout process, it may be possible to reconstruct changes in other sources of aerosol variability. Because this requires quantifying small deviations from a logarithmic process, such reconstructions must contend with uncertainty in that process, particularly in the scavenging efficiency.

Conclusions

Precipitation in the mid-latitudes is the principal barrier to aerosols reaching the poles. The hydrologic cycle drives concomitant variability in the dust, sea-salt and water isotope proxies and dominates the relationships between them at all timescales longer than several centuries. The rainout process explains the magnitude of variability in both terrestrial and marine-sourced aerosols and leads to a coherent view of the global pattern of dust changes across glacial cycles.

Our findings have important implications for the interpretation of aerosol proxy records and past climate. For example, the use of sea-salt records from ice cores as a proxy for sea ice extent has been widely debated (for example, refs [9,19]). We suggest that rather than faithfully recording such changes, the ice-core records of sea-salt variability primarily reflect changes in the strength of the hydrologic cycle. Similarly, changes in iron concentration in ice cores, which vary along with other dust proxies[9], have been used to infer the importance of iron fertilization in Southern Ocean productivity and CO_2 uptake[46]. Our results suggest that these Antarctica-based constraints overestimate the changes in iron delivery to the Southern Ocean.

Understanding the global spatial pattern of aerosol changes, particularly dust, is important to understanding past radiative forcing due to changes in aerosol optical depth. If dust source emission changes were the primary driver of the ice-core aerosol records, then orders-of-magnitude change in aerosol concentrations would be implied at all latitudes between glacial and interglacial periods. In contrast, our analysis suggests that due to the rainout effect, changes in aerosol concentrations were comparatively muted at lower latitudes, but strongly amplified toward the poles. The accompanying pattern of radiative forcing (Supplementary Information) may have important implications for how the climate system changed between the last glacial period and today.

Methods

Methods, including statements of data availability and any associated accession codes and references, are available at https://doi.org/10.1038/s41561-018-0210-9.

Received: 13 March 2018; Accepted: 18 July 2018;
Published online: 10 September 2018

References

1. Dansgaard, W. Stable isotopes in precipitation. *Tellus* **16**, 436–468 (1964).
2. Merlivat, L. & Jouzel, J. Global climatic interpretation of the deuterium-oxygen 18 relationship for precipitation. *J. Geophys. Res. Oceans* **84**, 5029–5033 (1979).
3. Jouzel, J. et al. Validity of the temperature reconstruction from water isotopes in ice cores. *J. Geophys. Res. Oceans* **102**, 26471–26487 (1997).
4. Legrand, M. R. & Delmas, R. J. Soluble impurities in four Antarctic ice cores over the last 30 000 years. *Ann. Glaciol.* **10**, 116–120 (1988).
5. Alley, R. et al. Changes in continental and sea-salt atmospheric loadings in central Greenland during the most recent deglaciation: model-based estimates. *J. Glaciol.* **41**, 503–514 (1995).
6. Wolff, E. & Bales, R. (eds) *Chemical Exchange between the Atmosphere and Polar Snow* Vol. 43 (NATO ASI subseries I, Springer, Berlin, 1996).
7. Petit, J.-R., Briat, M. & Royer, A. Ice age aerosol content from East Antarctic ice core samples and past wind strength. *Nature* **293**, 391–394 (1981).
8. Fischer, H. et al. Reconstruction of millennial changes in dust emission, transport and regional sea ice coverage using the deep EPICA ice cores from the Atlantic and Indian Ocean sector of Antarctica. *Earth Planet. Sci. Lett.* **260**, 340–354 (2007).
9. Wolff, E. W. et al. Southern Ocean sea-ice extent, productivity and iron flux over the past eight glacial cycles. *Nature* **440**, 491–496 (2006).
10. Delmonte, B., Petit, J. & Maggi, V. Glacial to Holocene implications of the new 27000-year dust record from the EPICA Dome C (East Antarctica) ice core. *Clim. Dynam.* **18**, 647–660 (2002).
11. Lambert, F. et al. Dust-climate couplings over the past 800,000 years from the EPICA Dome C ice core. *Nature* **452**, 616–619 (2008).
12. McGee, D., Broecker, W. S. & Winckler, G. Gustiness: the driver of glacial dustiness? *Quaternary Sci. Rev.* **29**, 2340–2350 (2010).
13. Andersen, K. K., Armengaud, A. & Genthon, C. Atmospheric dust under glacial and interglacial conditions. *Geophys. Res. Lett.* **25**, 2281–2284 (1998).
14. Li, F. et al. Toward understanding the dust deposition in Antarctica during the Last Glacial Maximum: sensitivity studies on plausible causes. *J. Geophys. Res. Atmos.* **115**, D24120 (2010).
15. Sugden, D. E., McCulloch, R. D., Bory, A. J. M. & Hein, A. S. Influence of Patagonian glaciers on Antarctic dust deposition during the last glacial period. *Nature Geosci.* **2**, 281–285 (2009).
16. Bauer, E. & Ganopolski, A. Aeolian dust modeling over the past four glacial cycles with CLIMBER-2. *Global Planet. Change* **74**, 49–60 (2010).
17. Delmonte, B. et al. Aeolian dust in East Antarctica (EPICA-Dome C and Vostok): provenance during glacial ages over the last 800 kyr. *Geophys. Res. Lett.* **35**, L07703 (2008).
18. Albani, S., Mahowald, N. M., Delmonte, B., Maggi, V. & Winckler, G. Comparing modeled and observed changes in mineral dust transport and deposition to Antarctica between the Last Glacial Maximum and current climates. *Clim. Dynam.* **38**, 1731–1755 (2012).
19. Petit, J.-R. & Delmonte, B. A model for large glacial–interglacial climate-induced changes in dust and sea salt concentrations in deep ice cores (central Antarctica): palaeoclimatic implications and prospects for refining ice core chronologies. *Tellus B* **61**, 768–790 (2009).
20. Rankin, A., Auld, V. & Wolff, E. Frost flowers as a source of fractionated sea salt aerosol in the polar regions. *Geophys. Res. Lett.* **27**, 3469–3472 (2000).
21. Curran, M., Wong, G., Goodwin, I., van Ommen, T. & Vance, T. Estimate of sea salt sources to Antarctica: an alternative interpretation of the EPICA sea salt record? In *Proc. European Geosciences Union General Assembly 2008* 1607-7962/gra/EGU2008-A-07581 (Vol. 10, Geophysical Research Abstracts series, European Geosciences Union, Copernicus, 2008).
22. WAIS Divide Project Members. Onset of deglacial warming in West Antarctica driven by local orbital forcing. *Nature* **500**, 440–444 (2013).
23. WAIS Divide Project Members. Precise interpolar phasing of abrupt climate change during the last ice age. *Nature* **520**, 661–665 (2015).
24. Lamy, F. et al. Increased dust deposition in the Pacific Southern Ocean during glacial periods. *Science* **343**, 403–407 (2014).
25. Markle, B. R. et al. Global atmospheric teleconnections during Dansgaard–Oeschger events. *Nature Geosci.* **10**, 36–40 (2017).
26. Mahowald, N. M. et al. Change in atmospheric mineral aerosols in response to climate: last glacial period, preindustrial, modern, and doubled carbon dioxide climates. *J. Geophys. Res. Atmos.* **111**, D10202 (2006).
27. Albani, S. et al. Improved dust representation in the Community Atmosphere Model. *J. Adv. Model. Earth Syst.* **6**, 541–570 (2014).
28. Kohfeld, K. E. & Harrison, S. P. DIRTMAP: the geological record of dust. *Earth-Sci. Rev.* **54**, 81–114 (2001).
29. Harrison, S. P., Kohfeld, K. E., Roelandt, C. & Claquin, T. The role of dust in climate changes today, at the Last Glacial Maximum and in the future. *Earth-Sci. Rev.* **54**, 43–80 (2001).
30. Anderson, R. F. et al. Biological response to millennial variability of dust and nutrient supply in the Subantarctic South Atlantic Ocean. *Philos. Trans. Roy. Soc. A* **372**, 20130054 (2014).
31. Yung, Y. L., Lee, T., Wang, C.-H. & Shieh, Y.-T. Dust: a diagnostic of the hydrologic cycle during the Last Glacial Maximum. *Science* **271,** 962–963 1996).
32. Tegen, I. & Fung, I. Modeling of mineral dust in the atmosphere: sources, transport, and optical thickness. *J. Geophys. Res. Atmos.* **99**, 22897–22914 (1994).
33. Sodemann, H. & Stohl, A. Asymmetries in the moisture origin of Antarctic precipitation. *Geophys. Res. Lett.* **36**, L22803 (2009).
34. Ciais, P. & Jouzel, J. Deuterium and oxygen 18 in precipitation: isotopic model, including mixed cloud processes. *J. Geophys. Res. Atmos.* **99**, 16793–16803 (1994).
35. Criss, R. E. *Principles of Stable Isotope Distribution* (Oxford University Press, Oxford, 1999).
36. Kaufman, Y. J., Tanré, D. & Boucher, O. A satellite view of aerosols in the climate system. *Nature* **419**, 215–223 (2002).
37. Kalnay, E. et al. The NCEP/NCAR 40-year reanalysis project. *Bull. Am. Meteorol. Soc.* **77**, 437–471 (1996).
38. Cuffey, K. M. et al. Deglacial temperature history of West Antarctica. *Proc. Natl Acad. Sci. USA* **113**, 14249–14254 (2016).
39. Otto-Bliesner, B. L. et al. Last Glacial Maximum and Holocene climate in CCSM3. *J. Clim.* **19**, 2526–2544 (2006).
40. Masson-Delmotte, V. et al. Past and future polar amplification of climate change: climate model intercomparisons and ice-core constraints. *Clim. Dynam.* **26**, 513–529 (2006).
41. De Angelis, M., Steffensen, J. P., Legrand, M., Clausen, H. & Hammer, C. Primary aerosol (sea salt and soil dust) deposited in Greenland ice during the last climatic cycle: comparison with East Antarctic records. *J. Geophys. Res. Oceans* **102**, 26681–26698 (1997).
42. Fischer, H., Siggaard-Andersen, M.-L., Ruth, U., Röthlisberger, R. & Wolff, E. Glacial/interglacial changes in mineral dust and sea-salt records in polar ice cores: sources, transport, and deposition. *Rev. Geophys.* **45**, RG1002 (2007).
43. Augustin, L. et al. Eight glacial cycles from an Antarctic ice core. *Nature* **429**, 623–628 (2004).
44. Kienast, S., Winckler, G., Lippold, J., Albani, S. & Mahowald, N. Tracing dust input to the global ocean using thorium isotopes in marine sediments: ThoroMap. *Global Biogeochem. Cycles* **30**, 1526–1541 (2016).
45. Rasmussen, S. O. et al. A stratigraphic framework for abrupt climatic changes during the Last Glacial period based on three synchronized Greenland ice-core records: refining and extending the INTIMATE event stratigraphy. *Quaternary Sci. Rev.* **106**, 14–28 (2014).
46. Sigman, D. M., Hain, M. P. & Haug, G. H. The polar ocean and glacial cycles in atmospheric CO_2 concentration. *Nature* **466**, 47–55 (2010).

Acknowledgements

We thank J. P. Steffensen for initial inspiration for this study and discussion. We thank M. Sigl, O. Maselli, R. Rhodes, D. Pasteris, L. Layman and others in the Ultra-Trace Chemistry Laboratory at the Desert Research Institute for assistance in developing the nssCa and ssNa records. We acknowledge grants from the US National Science Foundation Division of Polar Programs (0537930 and 1043092 to E.J.S., 0839093 and 1142166 to J.R.M. and 1405204 to G.W.). G.W. was supported by a Senior Fellowship from the Center for Climate and Life.

Author contributions

B.R.M. conceived the study and carried out the primary analyses. B.R.M., G.H.R. and E.J.S. developed the rainout model. G.W. provided analyses comparing marine and ice-core records. J.R.M. provided the ice-core impurity measurements. B.R.M. led the manuscript writing, with assistance from E.J.S. and G.H.R. All authors discussed results and contributed to the manuscript.

Competing interests

The authors declare no competing interests.

Additional information

Supplementary information is available for this paper at https://doi.org/10.1038/s41561-018-0210-9.

Reprints and permissions information is available at www.nature.com/reprints.

Correspondence and requests for materials should be addressed to B.R.M.

Publisher's note: Springer Nature remains neutral with regard to jurisdictional claims in published maps and institutional affiliations.

Methods

Data. *Water isotopes.* WDC $\delta^{18}O$ was measured at IsoLab, University of Washington, and published previously[22,25]. Measurement techniques are described in ref. [25]. Measurements were made at 0.5 m depth-averaged resolution, using laser spectroscopy (Picarro L2120-*i* analyser). Data are reported relative to Vienna Standard Mean Ocean Water (VSMOW) and normalized to Standard Light Antarctic Precipitation (SLAP). Measurement resolution is generally better than 40 yr per sample for the 67 ka record, with a mean temporal resolution of 17.2 yr per sample between 10 ka and 67 ka. Measurement uncertainties are less than 0.08‰ (1 s.d.) for $\delta^{18}O$.

Aerosols. The marine-sourced and non-marine-sourced components of the sodium and calcium impurities of ice are, respectively, ssNa and nssCa. WDC ice impurities were measured at the Ultra-Trace Chemistry Laboratory at the Desert Research Institute, using a continuous flow system and inductively coupled plasma mass spectrometry[47,48]. While parts of these records have been published previously[22,23,48,49], the full records are presented here. The effective sampling resolution is ~1 cm. Because the elements Ca and Na appear in both mineral dust and sea salts, those ions alone are not unique identifiers of the aerosols of interest. We use standard calculations to isolate the sea-salt component of the sodium and the non-sea-salt component of the calcium records. These are calculated by accounting for Na/Ca mass ratios of 26.3 for marine aerosols and 0.562 for average crust composition[50,51].

Aerosol amplification factors, presented throughout, represent normalized changes in concentration for the WDC record. We also present amplification factors of aerosol fluxes for EDC and the EPICA Dronning Maud Land ice core (EDML). Because of the high accumulation rate in West Antarctica, changes in WDC aerosol concentrations are a faithful representation of past changes in the overlying atmospheric aerosol concentration, whereas the flux is a more appropriate quantification for atmospheric concentration at low accumulation sites such as those of EDC and EDML[5,42]. The difference between flux and concentration is at most a factor of two at all sites, owing to changes in accumulation[22,42,52], a minor consideration given the orders-of-magnitude aerosol change observed in the records. It is interesting to note, however, that at the WDC site, the correlation between $\delta^{18}O$ and accumulation is high at orbital timescales, but degrades at millennial and shorter timescales[52] (Supplementary Information). This relationship is largely assumed to be fixed at many East Antarctic sites, where accumulation may not be calculated independently from water isotope records. The assumption that the relationship between water isotopes and accumulation is fixed may obscure true variability in calculated East Antarctic aerosol fluxes, although it is probably unimportant for the timescales investigated here.

Simple atmospheric transport, water isotope and aerosol model. Here, we describe the framework of the simple rainout model. We are interested in understanding centennial and longer variability in the water isotope and aerosol records. The relevant climate variables are well mixed and roughly zonally symmetric in the Southern Hemisphere at these timescales. We assume only that the mean transport depends on the mean climate and that the statistics are reasonably stationary.

We consider air transported from the surface in the mid-latitudes toward the pole. We assume pseudoadiabatic cooling during transport following the meridional temperature gradient. The temperature dependence of the moisture content of the atmosphere is described by the Clausius–Clapeyron relation:

$$\frac{1}{e_s}\frac{\mathrm{d}e_s}{\mathrm{d}T} = \frac{L}{\overline{R}T^2} \tag{1}$$

where the change in saturated vapour pressure, e_s, with temperature, T, depends on the latent heat, L, and specific gas constant, $\overline{R}$ Equation (1) and the assumption of pseudoadiabatic cooling together describe the changes with temperature of the saturated mixing ratio, r_s. We account for mixed ice and liquid in the atmosphere and the difference in the associated vapour pressures. Our results are robust to the details of the mixed-phase nature of the pathway, as well as the pseudoadiabatic assumption; an isobaric assumption leads to the same conclusions.

We assume that as the air cools, moisture is removed owing to the temperature-driven changes in the saturated mixing ratio: all moisture above saturation (or supersaturation) is immediately removed as precipitation. This is a simplified view of large-scale precipitation resulting from moisture transport down a temperature gradient and follows previous moisture transport frameworks used to understand ice-core records[1,2,35].

The moisture removal, water isotope distillation and aerosol removal equations are integrated along temperature profiles and projected onto a latitudinal grid. We use Euler numerics in both the water isotope and aerosol models, $\frac{\mathrm{d}y_i}{\mathrm{d}x_i} \approx \frac{y_i - y_{i-1}}{x_i - x_{i-1}}$, with sufficiently small $\Delta x = x_i - x_{i-1}$, where y is the dependent variable, x is a grid variable such as latitude or temperature, and subscript i refers to the ith element of the vectors y and x.

Aerosols are transported from source latitudes toward the poles. In the Southern Hemisphere, we use an effective mean dust emission latitude of 35° S and an effective sea-salt emission latitude of 60° S, corresponding to idealized South American and Southern Ocean sources, respectively, and in line with satellite observations[36] and models[18].

The amount of aerosol removed from the atmosphere, by either wet or dry removal, depends on the concentration of aerosol in the atmosphere, $\frac{\mathrm{d}C}{\mathrm{d}x} \propto C$ (C is the atmospheric concentration of aerosol), which leads to the inherent exponential decay of aerosol concentrations as they are transported from the source:

$$C = C_0 \mathrm{e}^{-\frac{x}{\chi}} \tag{2}$$

where C_0 is the initial source concentration, x is a grid variable such as time, distance or latitude, and χ is a characteristic length scale or timescale determined by the combined wet and dry removal.

The relationship between the concentration of an aerosol in the atmosphere, C_{air} (which by convention has units $\frac{\text{g aerosol}}{\text{cm}^3}$), and that in precipitation, C_{precip} (in units $\frac{\text{g aerosol}}{\text{g precipitation}}$), resulting from scavenging and rainout, is quantified by the mass-scavenging ratio[53]:

$$\omega = \frac{C_{precip}}{C_{air}}\rho_{air} \tag{3}$$

where ρ_{air} is the density of air, and ω has units $\frac{\text{g aerosol}}{\text{g precipitation}} \div \frac{\text{g aerosol}}{\text{g air}}$ (ref. [6]).

The change in aerosol concentration of the atmosphere owing to wet removal depends on C_{air}, ω and the amount of moisture removed, $-P$ (in units $\frac{\text{g precipitation}}{\text{g air}}$), where the negative sign denotes that moisture is leaving the air. Thus, the dependence of aerosol concentration on latitude, ϕ, is determined by the temperature dependence of the saturated mixing ratio, $\frac{\mathrm{d}r_s}{\mathrm{d}T}$, and the change in temperature with latitude, $\frac{\mathrm{d}T}{\mathrm{d}\phi}$:

$$\left(\frac{\mathrm{d}C_{air}}{\mathrm{d}\phi}\right)_{wet} = -PC_{precip}\rho_{air} = \frac{\mathrm{d}r_s}{\mathrm{d}T}\frac{\mathrm{d}T}{\mathrm{d}\phi}\omega C_{air} \tag{4}$$

To assess changes in aerosol concentrations due solely to wet removal, equation (4) is integrated from the initial source latitude, ϕ_0, and C_0 to the final deposition latitude, yielding an exponential decay equation similar to equation (2).

The aerosol mass-scavenging ratios for calcium and sodium are measured empirically and of orders 1×10^3 to 2×10^3, in units of $\frac{\text{g aerosol}}{\text{g precipitation}} \div \frac{\text{g aerosol}}{\text{g air}}$. We use central values (1,400 for nssCa and 1,500 for ssNa) from a compilation of empirical measurements of this parameter (Supplementary Information). We test the sensitivity of the model to uncertainty in this parameter (Fig. 3b and Supplementary Information).

We are primarily concerned with changes in aerosol concentration due to wet removal. For completeness, a dry deposition term may be added to equation (4):

$$\left(\frac{\mathrm{d}C_{air}}{\mathrm{d}\phi}\right)_{dry} = C_{air}v_{dry}\frac{\mathrm{d}t}{\mathrm{d}\phi} = \frac{C_{air}v_{dry}}{w(\phi)} \tag{5}$$

in which additional dry removal of an aerosol depends on its concentration, a dry deposition rate, v_{dry}, and the amount of time spent transiting a latitude band, which depends on the meridional wind speed, $w(\phi)$, a function of latitude. Integrating the combined wet and dry removal across latitude gives

$$C(\phi) = C_0 \mathrm{e}^{\int_{\phi_0}^{\phi}\left(\omega\frac{\mathrm{d}r_s}{\mathrm{d}T}\frac{\mathrm{d}T}{\mathrm{d}\theta} + \frac{v_{dry}}{w(\theta)}\right)\mathrm{d}\theta} \tag{6}$$

Once integrated, the first term in the exponent is the scavenging efficiency multiplied by the integrated precipitation, $-\omega\int P(\phi)$, or simply $-\omega(q_0 - q(\phi))$, where q is the atmospheric moisture and the negative sign reflects removal of the moisture from the atmosphere. The second term in the exponent is the integrated dry deposition rate, which, for now, we call $-D$. If we use the prime symbol to denote a new climate state, then, at a given high-latitude site, the aerosol amplification factor is

$$\frac{C'}{C} = \frac{C_0' \mathrm{e}^{-\left(\omega\int P(\phi)' + D'\right)}}{C_0 \mathrm{e}^{-\left(\omega\int P(\phi) + D\right)}} \tag{7}$$

Previous work suggests that dry deposition processes and transport efficiency did not change substantially between climate states[8]. If v_{dry} and $w(\phi)$ are constant, and assuming fixed source emission, the amplification factor of aerosol concentrations between climate states depends on changes in integrated precipitation only:

$$\frac{C'}{C} = \mathrm{e}^{-\omega\left(\int P(\phi)' - \int P(\phi)\right)} \tag{8}$$

The aerosols and water that reach an ice-core site are transported along overlapping latitudinal pathways that obey the same thermodynamics. We use

an effective moisture source latitude of 45° S for the WDC site, as estimated by a moisture-tagged general circulation model experiment[25], and initialize water isotopes according to representative source region conditions. Water isotopes are distilled to the deposition site following well-established fractionation equations[1,2,34,35]. We use a Rayleigh-type distillation model[1,2,35,54] in which

$$\frac{\mathrm{d}\ln(R)}{\mathrm{d}\ln(f)} = \alpha - 1 \tag{9}$$

where R and α are the isotopic ratio and fractionation factor, respectively. The variable f is the fraction of initial water vapour remaining in the air parcel, $f = \frac{q(\phi)}{q_0} = \frac{r_s(\phi)}{r_s(\phi_0)}$.

We account for both equilibrium and non-equilibrium fractionation of water isotopes, mixed ice and liquid phases, and source region conditions, and use a parameterized supersaturation. While similar to previous models[34,55], we make several improvements, including updated fractionation factors[25,56,57], consistent saturation and supersaturation conditions between the water isotope fractionation and the physical moisture pathway, temperature dependence of liquid/ice-phase mixing on the basis of satellite measurements[58], which together result in fidelity to modern δ^{18}O, δD (the normalized deuterium and hydrogen ratio in the water, calculated along with δ^{18}O), and temperature observations[59].

The fundamental origin of the negative-exponential relationship between aerosols and water isotopes can be seen by considering a simplified scenario. Using the definition of a delta value, assuming an initial isotopic value of the vapour, δ_0, and assuming constant α, equation (9) can be integrated to find the delta value of the vapour at any point along the cooling path:

$$\delta = \delta_0 \left(\frac{q}{q_0}\right)^{\alpha-1} \tag{10}$$

Considering a change between climate states, then

$$\Delta\delta = \delta' - \delta = \delta_0 \left(\left(\frac{q'}{q_0'}\right)^{\alpha-1} - \left(\frac{q}{q_0}\right)^{\alpha-1} \right) \tag{11}$$

With equations (11) and (8), and recalling that the Clausius–Clapeyron relation is a nonlinear function of temperature, we can compare $\Delta\delta$ and $\log\left(\frac{C'}{C}\right)$ at a site for a change in climate mean state. As mean temperature increases, integrated precipitation increases (owing to Clausius–Clapeyron), and thus $\log\left(\frac{C'}{C}\right)$ decreases. Concomitantly, as temperature increases, so do $\frac{q}{q_0}$ (also a result of Clausius–Clapeyron) and $\Delta\delta$. Thus, $\Delta\delta$ and $\log\left(\frac{C'}{C}\right)$ are inversely related at high-latitude sites for a change in mean climate temperature. The full model accounts for temperature-driven changes in α, mixed ice/liquid phases in the parcel, equilibrium and kinetic fractionation, supersaturation, isotope source effects and changes in $\frac{\mathrm{d}T}{\mathrm{d}\phi}$, all of which contribute to the results. The negative-exponential relationship, however, is more fundamental than any of these effects.

Data availability. All WDC data presented here will be available at the United States Antarctic Program Data Center. The WDC water isotope ratio data are identified by https://doi.org/10.17911/S9MW2F and the impurity data by https://doi.org/10.15784/601008.

Code availability. MATLAB code for the simple model is available from the corresponding author upon request.

References

47. McConnell, J. R., Lamorey, G. W., Lambert, S. W. & Taylor, K. C. Continuous ice-core chemical analyses using inductively coupled plasma mass spectrometry. *Environ. Sci. Tech.* **36**, 7–11 (2002).
48. McConnell, J. R. et al. Synchronous volcanic eruptions and abrupt climate change ~17.7 ka plausibly linked by stratospheric ozone depletion. *Proc. Natl Acad. Sci. USA* **114**, 10035–10040 (2017).
49. Jones, T. et al. Water isotope diffusion in the WAIS Divide ice core during the Holocene and last glacial. *J. Geophys. Res. Earth Surf.* **122**, 290–309 (2017).
50. Bowen, H. J. M. (ed.) *Environmental Chemistry* Vol. 3 (Royal Society of Chemistry, London, 1984).
51. Röthlisberger, R. et al. Dust and sea salt variability in central East Antarctica (Dome C) over the last 45 kyrs and its implications for southern high-latitude climate. *Geophys. Res. Lett.* **29**, 1963 (2002).
52. Fudge, T. et al. Variable relationship between accumulation and temperature in West Antarctica for the past 31,000 years. *Geophys. Res. Lett.* **43**, 3795–3803 (2016).
53. Davidson, C. et al. Seasonal variations in sulfate, nitrate and chloride in the Greenland ice sheet: relation to atmospheric concentrations. *Atmos. Environ.* **23**, 2483–2493 (1989).
54. Rayleigh, L. LIX. On the distillation of binary mixtures. *Philos. Mag.* **4**, 521–537 (1902).
55. Kavanaugh, J. L. & Cuffey, K. M. Space and time variation of δ^{18}O and δD in Antarctic precipitation revisited. *Global Biogeochem. Cycles* **17**, 1017 (2003).
56. Uemura, R., Matsui, Y., Yoshimura, K., Motoyama, H. & Yoshida, N. Evidence of deuterium excess in water vapor as an indicator of ocean surface conditions. *J. Geophys. Res. Oceans* **113**, D19114 (2008).
57. Lamb, K. D. et al. Laboratory measurements of HDO/H_2O isotopic fractionation during ice deposition in simulated cirrus clouds. *Proc. Natl Acad. Sci. USA* **114**, 5612–5617 (2017).
58. Hu, Y. et al. Occurrence, liquid water content, and fraction of supercooled water clouds from combined CALIOP/IIR/MODIS measurements. *J. Geophys. Res. Atmos.* **115**, D00H34 (2010).
59. Markle, B. R. *Climate Dynamics Revealed in Ice Cores: Advances in Techniques, Theory, and Interpretation*. PhD thesis, Univ. Washington (2017).

nature geoscience

SUPPLEMENTARY INFORMATION

https://doi.org/10.1038/s41561-018-0210-9

In the format provided by the authors and unedited.

Concomitant variability in high-latitude aerosols, water isotopes and the hydrologic cycle

Bradley R. Markle[1,2]*, Eric J. Steig[1], Gerard H. Roe[1], Gisela Winckler[3] and Joseph R. McConnell[4]

[1]Department of Earth and Space Sciences, University of Washington, Seattle, WA, USA. [2]Earth Research Institute, University of California Santa Barbara, Santa Barbara, CA, USA. [3]Lamont-Doherty Earth Observatory of Columbia University, Palisades, NY, USA. [4]Desert Research Institute, Reno, NV, USA. *e-mail: marklebr@uw.edu

SUPPLEMENTARY MATERIALS: CONCOMITANT VARIABILITY IN HIGH-LATITUDE AEROSOLS, WATER-ISOTOPES, AND THE HYDROLOGIC CYCLE

BRADLEY R. MARKLE[1,2*]

ERIC J. STEIG[1]

GERARD H. ROE[1]

GISELA WINCKLER[3]

JOSEPH R. MCCONNELL[4]

[1]*Department of Earth and Space Sciences, University of Washington, Seattle, Washington 98195, USA*

[2]*Earth Research Institute, University of California Santa Barbara, Santa Barbara, CA 93106-3060, USA*

[3]*Lamont-Doherty Earth Observatory of Columbia University, Palisades, NY 10964, USA*

[4]*Desert Research Institute, Reno, NV 89512, USA*

**Correspondence to: marklebr@uw.edu*

Table of Contents

S1. Sensitivity of simple rainout model

We investigate sensitivities in our model to uncertainties and plausible variability in the factors related to the wet removal of aerosols, including the mass-scavenging ratio, initial source concentration, source emission latitude, and polar amplification.

S1.1. **Mass-Scavenging Ratio.** The mass-scavenging ratio is empirically derived and relates the concentration of an aerosol in precipitation to the concentration in air[1],

$$\omega = \frac{C_{precip}}{C_{air}} \rho_{air} \tag{S1}$$

where ρ_{air} is the density of air[2]. We use estimates for each aerosol based on a compilation of scavenging ratios measured across a range of mid and high latitude environments (discussed in Section S6 and summarized in Table S1). Both calcium and sodium aerosols have a mass-scavenging ratio of magnitude 1-2 $\times 10^3$ $\frac{\text{g aerosol}}{\text{g precipitation}} \div \frac{\text{g aerosol}}{\text{g air}}$, though the precise values are uncertain. Reasonable estimates (1400 for nssCa and 1500 for ssNa) from our compilation account for the entire range of variability observed in both aerosols in the WDC record.

Because the mass-scavenging ratio is in the exponent of the rainout equations, uncertainty in this parameter could be important. This uncertainty may reflect inherent difficulty in measuring the scavenging parameter or true variance that depends on climate and microphysics. We test the sensitivity of our model results for calcium to a range of mass-scavenging ratios (1400 ± 500) as shown in Figure 3. The sensitivity of sodium is similar.

It is important to note that all interpretations of the variability in high-latitude aerosols are subject to the uncertainty in the scavenging efficiency. If the the mass-scavenging ratio were less than our estimates, some amount of variability in the aerosol records could

be accounted for by other sources of variability, such as changes in source emission. However, if the scavenging coefficient were greater, an equally likely scenario, then source emission changes of the opposite sign would be implied.

S1.2. **Initial source concentration.** Changes in aerosol source emission lead to linear amplification of aerosols along the deposition path. Figure 3c shows the spread in the modeled relationship between water isotopes and aerosols associated with 1/3- to 3-fold changes in initial aerosol concentration at any instant in time. In Figure S1 we compare the measured nssCa variability in WDC to predicted nssCa variability based solely on the modeled relationship between δ^{18}O and nssCa and the measured δ^{18}O in WDC. The log of the real and modeled WDC nssCa are extremely well correlated, $r = 0.91, p < 0.01$, indicating the model can explain >80% of the variance in the nssCa record. We also show the time series of predicted nssCa if source emissions either doubled or halved from the LGM to 10 ka. Temporal changes in source strength will alter the shape of the relationship between water isotopes and aerosols in Figure 3. We cannot rule out 2-3 fold increases or decreases of source emission strength based on the ice-core data alone; such changes are within the spread of observations in Figure 3 and within the uncertainty of other model parameters, particularly the scavenging efficiency.

S1.3. **Source-emission latitude.** The latitude of aerosol source-emission determines the influence of the rainout effect. Aerosols emitted from a lower latitude source must be transported through a greater temperature gradient to reach Antarctica, and thus experience more integrated rainout and greater amplification due to changes in rainout, than those emitted from higher latitudes. Several lines of evidence indicate South America is the dominant source of Antarctic dust[3;4]. The CESM Large Ensemble Experiment[5] shows dust aerosol burdens to peak between 30° and 35°S (see below), while other studies highlight South American dust-production regions between 37°S and 42°S[4]. For Southern Hemisphere sea-salts, satellite observations and models[6] indicate that the dominant source region is the Southern Ocean between 50° and 65°S, though there may be contribution from higher latitude sea ice as well (e.g ref[7]).

The initial source emission of a given aerosol may be distributed over a range of latitude. We approximate aerosol emissions as originating from a single effective source-latitude, ϕ_0, using 35°S for terrestrial dust and 60°S for sea salt. These effective source-latitudes may be uncertain, may be variable within a mean state, and may change between mean states. In Figure 3d we show the range of variability in aerosol amplification factor associated with a +10° and -10° variation in the source latitude of calcium. If source latitudes for dust, sea salts, or moisture changed with climate, the slope of the negative exponential isotope-aerosol relationship could be altered. Small changes in source latitude (e.g.< 5°) could be difficult to detect as they may be within the noise of the records or within the uncertainty of other factors. We investigate the potential influence of source latitude changes on an 800 thousand year record of dust changes below.

The importance of a generic aerosol source-latitude to a particular site can be quantified by calculating a wet-removal weighting function which accounts for the integrated

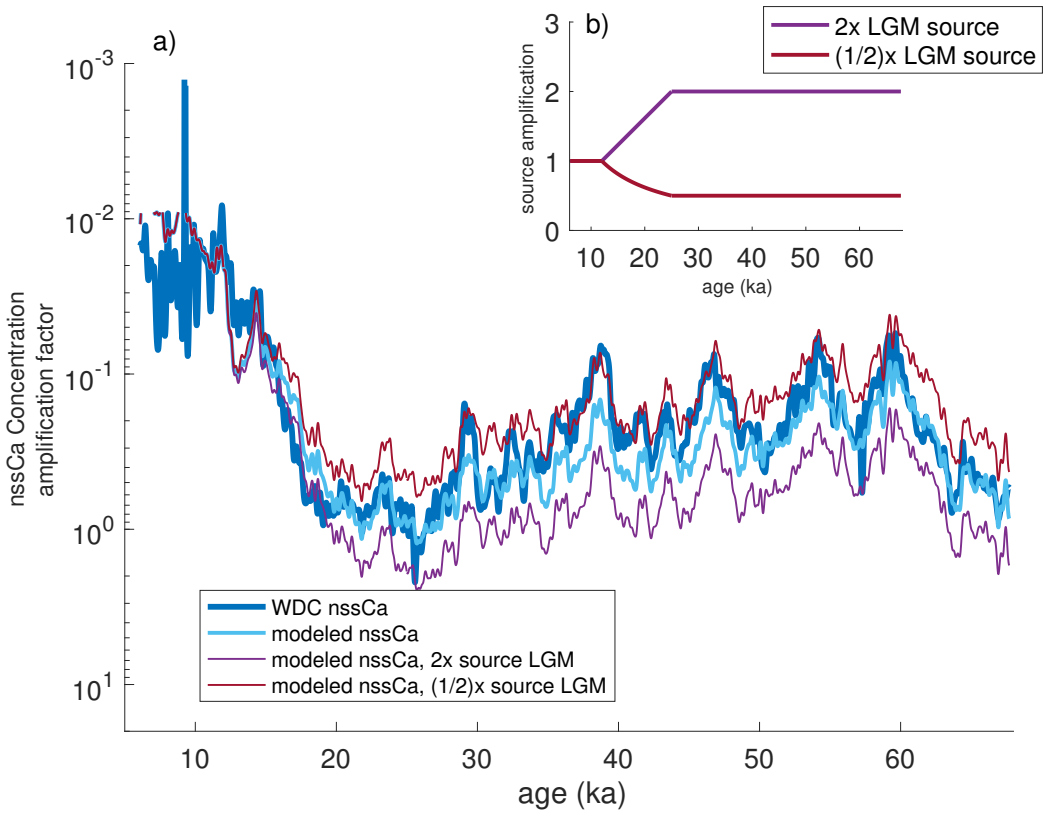

FIGURE S1. a) WDC nssCa record compared to the predicted variability based solely from the WDC δ^{18}O (low pass filtered, frequencies > $\frac{1}{300yrs}$ removed) and the rainout model. We also show the expected variability in the predicted in nssCa associated with a temporal increase or decrease in the initial source strength, C_0. Note inverted y-axis. b) The idealized temporal changes in C_0 are shown in the inset.

rainout experienced by an aerosol between all possible starting latitudes and the final latitude of deposition at an ice-core site. The perceived aerosol source region for a given site in Antarctica is the latitudinal distribution of aerosol emission convoluted with the wet-removal weighting function. In Figure S2a and b we show the wet-removal weighting function for Southern Hemisphere aerosols reaching 75°S, in linear and log-scale, respectively. The distribution is equal to the relative amount of aerosol arriving at the final ice-core site (e.g. 75°S) as a function of source latitude (with equal emission, C_0, at all latitudes). Hypothetical aerosols with an initial source-latitude at 75°S will have a weighting of 1, i.e. no removal. The weighting function decreases exponentially toward the equator. For reference, the latitudinal histogram of land area of Southern Hemisphere continents (South America, Africa, and Australia) are shown in Figure S2c and the area of the Southern Hemisphere oceans shown in Figure S2d. Emissions of terrestrial dust

and marine sea-salts depend on the available area of their respective sources, as well as other factors including production rates, wind speed, and entrainment.

A result of the wet-removal weighting function in Figure S2 is that the perceived aerosol source-latitude, from the perspective of an ice-core site, may be closer to the pole than the latitude of the mean or peak of the distribution of aerosol emission. This may give a natural explanation for why most Antarctic dust comes from South America rather than other potential sources like Australia and South Africa. By the time they reach Antarctica, aerosols emitted from 30°S, for example, may be reduced in concentration by orders of magnitude compared to those emitted from 40°S. Because South America extends more than 10° of latitude poleward than either Australia or South Africa, dust from South America would have an exponentially greater probability of reaching Antarctica, even if source emissions for each region were identical. Likewise, this effect, together with circulation patterns, can help explain why geochemical fingerprinting of LGM and interglacial dust deposited in Antarctica point to a southern South American provenance, perhaps as far south as 50°S (e.g. refs[8;9]), while paleoclimate modeling[4] and modern observations[10] suggest the peak dust emissions in South America are at lower latitudes. Higher latitude dust-production sources, such as Patagonian[8] and New Zealand glaciers, are likely more important to Antarctica than larger-area but lower-latitude sources.

S1.4. **Polar amplification.** Polar amplification is the change in the meridional temperature gradient, $\frac{dT}{d\phi}$, with mean climate. Estimates from models[11] and paleoclimate data[12] suggest that, since the LGM, the highest latitudes warmed on the order of 4°C for every degree of low latitude warming. Total glacial-interglacial change at WDC is estimated at about 10°C[13;14]. Results in Figure 3 are for a polar amplification of 4°C of high latitude warming per 1°C of equatorial warming, prescribed linearly with latitude. However, polar amplification in the real climate was not likely linear with latitude. During transport water, dust, and sea salts experience overlapping, but distinct, segments of the rainout pathway. Because of this, the relationships between the aerosols and water isotopes may record the spatial pattern of polar amplification.

We test the behavior of the rainout model to idealized spatial patterns of polar amplification (Figure S3). Importantly, global temperature change with no polar amplification would still result in large glacial-interglacial changes in Antarctic aerosols, and the negative-exponential relationship with water isotopes. Because the saturation vapor pressure scales nonlinearly with temperature, even equal temperature change at all latitudes leads to changes in the gradient of moisture and thus condensation and wet-removal of aerosols. However, a polar amplification of 4°C of high latitude warming per 1°C of equatorial warming, in line with evidence[11;12], more faithfully captures the relative slopes between ssNa and δ^{18}O and nssCa and δ^{18}O compared to warming without polar amplification. We calculate the zonal-mean pattern of polar amplification from the ECHAM4.6 GCM run under preindustrial and LGM boundary conditions[15;16], which is consistent with previous GCM modeling experiments (e.g. ref[11]). This pattern of polar amplification results curvature in the δ^{18}O-to-log(ssNa) and δ^{18}O-to-log(nssCa)

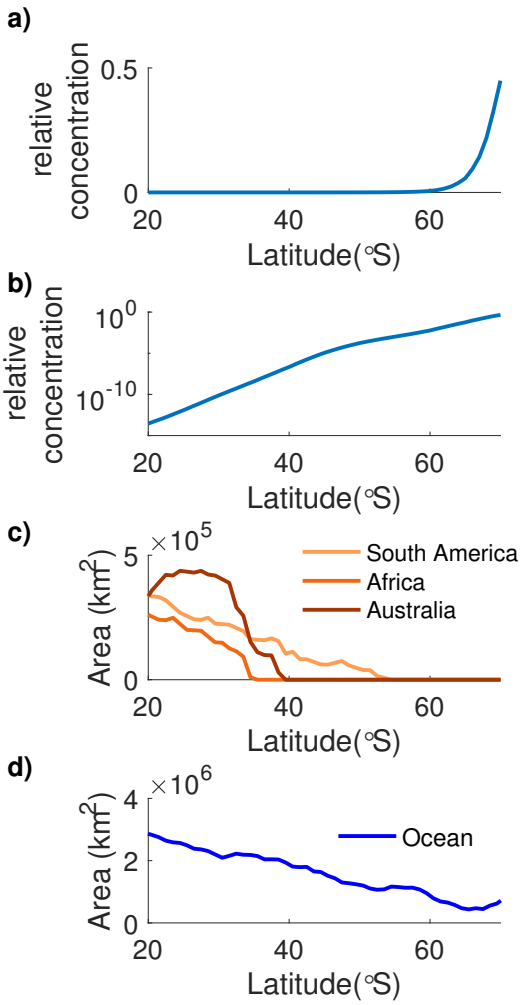

FIGURE S2. a) The wet-removal weighting function, with $\omega = 1700$, for equal emission from all Southern Hemisphere latitudes for aerosols reaching 75°S. b) same as a) but on a log axis. c) The land area as a function of latitude for the major Southern Hemisphere continents. d) Surface area as a function of latitude for the Southern Hemisphere oceans.

relationships and is distinct from the curvature resulting from polar amplification that is linear with latitude. This curvature comes from differences in the relative warming of overlapping latitudinal segments of the rainout path, and varies between ice-core sites. In Figure S3 we show the nssCa flux, ssNa flux, and δ^{18}O records from the East Antarctic EPICA Dome C (EDC) and EPICA Dronning Maud Land (EDML) ice-core records [17] in

addition to the records from WDC. The East Antarctic records show stronger curvature in the δ^{18}O-to-log(ssNa) relationship than the West Antarctic record. This result is similar to the relationships driven by the ECHAM4.6 pattern of polar amplification; colder sites show stronger curvature in the δ^{18}O-to-log(ssNa) relationship.

We next investigate the influence of temporal variability in the pattern of polar amplification on the aerosol-water isotope relationship. We use an energy balance model[18;19] to produce temperature profiles for a range of mean-state temperatures. We alter the physics in the model to produce different zonal-mean patterns of polar amplification, as well as patterns of polar amplification that change with mean temperature (and would thus be temporal changes in polar amplification in a changing climate, Figure S4).

In the energy balance model (EBM)[18;19] the spatial pattern of downward radiative forcing is specified, upward emission is parameterized based on a linearization with temperature, and horizontal heat transport is based on heat diffusion. All scenarios are initialized to match the modern meridional temperature gradient. The top-of-atmosphere radiative forcing is perturbed and the model allowed to come to equilibrium to produce different mean states. The physics of the horizontal transport is varied in our experiments to produce different patterns of polar amplification. We examine 1) horizontal heat transport driven by dry thermal diffusion; 2) heat transport driven by the down gradient diffusion of moist static energy (MSE)[18] rather than dry thermal energy; and 3) heat transport driven by MSE diffusion with the addition of an ice-albedo feedback, in which surface albedo changes with temperature (specifically the albedo is 0.3 for latitudes warmer than -10°C and 0.6 for those colder). We use the resulting suite of self-consistent pole-to-equator temperature gradients from each set of scenarios to drive the water-isotope and aerosol-rainout model. We test the sensitivity of the relationships between water-isotopes and aerosols under transient conditions with different patterns of polar amplification. In Scenario 1), simple dry diffusion leads to polar damping: for every degree of equatorial warming the poles experience a fraction of a degree. Scenarios 2) and 3) result in polar amplification with spatial patterns that change with the mean-state temperature.

The influence of the polar amplification scenarios on the relationship between water isotopes and nssCa and ssNa aerosols for an ice-core site at 80°S is shown in Figure S4. All patterns of polar amplification drive rainout that leads to a negative exponential relationship between aerosols and water isotopes. Further, we see that the nature of polar amplification and its temporal evolution is imprinted upon the nssCa-water isotope and ssNa-water isotope relationships. For example, in Scenario 3 the moving ice/albedo edge shifts the peak of polar amplification equatorward with a cooling climate. This evolving polar amplification changes the slope in the exponential δ^{18}O-to-nssCa relationship, in fact inverting the slight curvature seen in Scenario 1. The calcium records in the WDC, EDC, and EDML ice core all show curvature of this sign (Figure S3c). While it is not possible, from these tests alone, to uniquely ascribe the second derivative of the water-isotope-to-aerosol relationship in the ice-core records to polar amplification, our results

demonstrate that the spatial and temporal patterns of polar amplification are imprinted upon the relationships between these proxies.

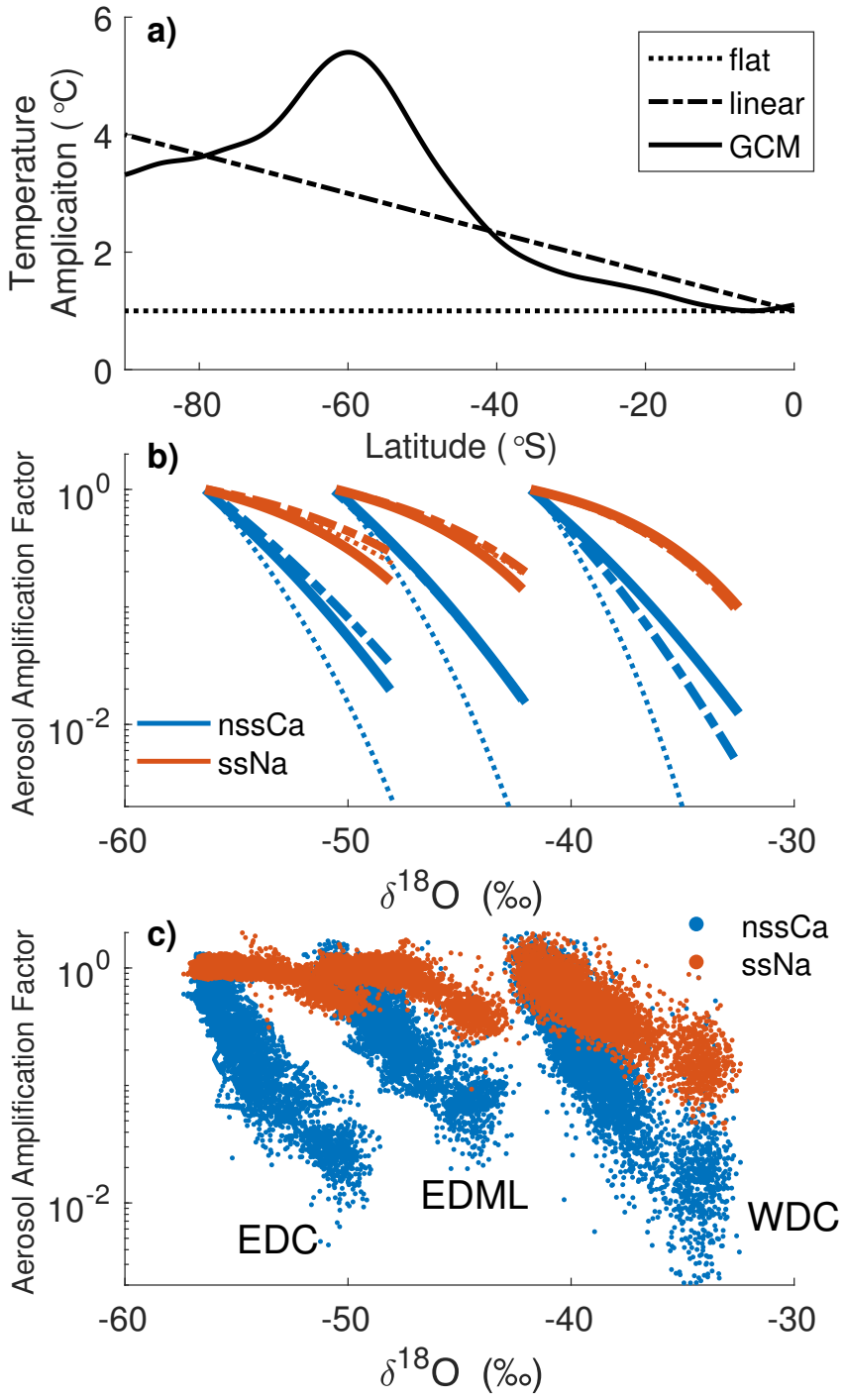

FIGURE S3. a) Three patterns of polar amplification (degree of warming per degree of equatorial warming). "Flat": equal warming at all latitudes. "Linear": linearly increasing amplification toward the pole. "GCM": pattern of warming from preindustrial-LGM ECHAM4.6 control runs. b) Relationship between modeled δ^{18}O, nssCa, and ssNa for three different patterns of polar amplification at three sites representative of the isotope values at WDC, EDML, and EDC. c) Relationship between δ^{18}O and nssCa (blue) and δ^{18}O and ssNa (red), for WDC, EDC, and EDML. Aerosol data are presented as amplification factors from the LGM. Aerosol data are amplification of concentration for WDC, and of flux for EDC and EDML.

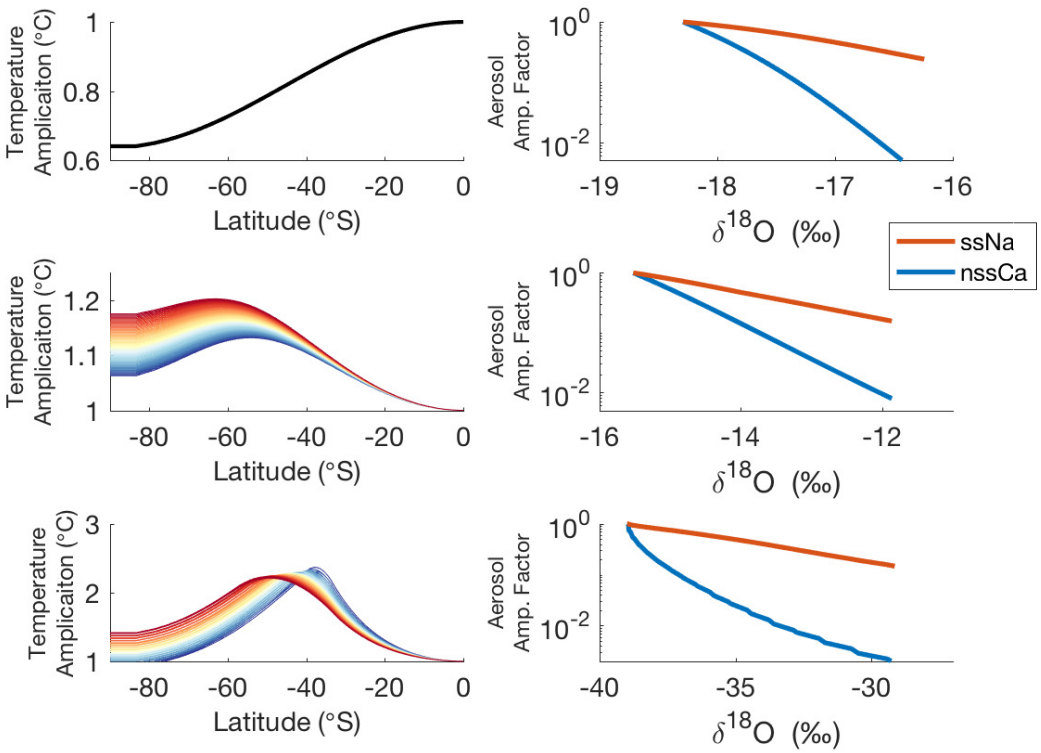

FIGURE S4. Influence of polar amplification on aerosol-water isotope relationships. The left panels show spatial patterns (degree of warming with latitude per degree of equatorial warming) from three different energy balance scenarios. Top: dry thermal diffusion (note this actually leads to polar damping of temperature change). Middle: moist thermal diffusion. The different colored lines reflect the spatial pattern of polar amplification with relative changes in global mean temperature. Red colors are warmer mean-state temperatures while blue colors are colder mean-state temperatures. Bottom: moist thermal diffusion with ice-albedo feedback. Colors represent relative change in global mean temperature. The right column shows the associated patterns of ssNa (red) and nssCa (blue) concentration change with water isotope change at 80°S. Note the changing curvature, particularly in nssCa.

S2. Timescales

Here we investigate the timescale dependence of the relationship between water isotopes and aerosols. In Figure S5, we show the relationship between the WDC δ^{18}O and log(nssCa) records filtered for different frequency bands of variability. We examine the following times scales: the full record (>40,000 to 10 yr periods); >10,000 yr; >1,000 yr; 10,000-1,000 yr; 5,000-1,000 yr; 2,000-500 yr; and <1,000 yr periods of variability. At all but the shortest periods (<1,000 yr), δ^{18}O and log(nssCa) are similarly well-correlated and with similar slopes. There is some indication of a steeper slope at the longest timescales, but the differences in slope are small.

The spectral coherence of WDC δ^{18}O and log(nssCa), as well as δ^{18}O and log(ssNa) (interpolated to even 10 yr/sample spacing), are shown in Figure S6. The records are significantly coherent from orbital to multi-centennial timescales. At periods shorter than multi-centennial the water-isotope and aerosol records are not significantly coherent. By comparison WDC δ^{18}O and local accumulation, for example, are not significantly coherent at timescales shorter than multi-millennial[20].

This analysis suggests that the same processes that drive the relationship between water isotopes and aerosols on glacial-interglacial timescales are the same as the process driving their relationship on millennial timescales. This leaves only a limited role for mechanisms driving aerosol variance that may have specific long timescales associated with them, such as Southern Hemisphere glacial activity or large-scale biome changes. This analysis does not suggest that those processes do not affect source emissions, only that their variance is not the dominant driver of the variance in the ice-core record. On shorter timescales, the water-isotope aerosol relationship is overwhelmed by other, unshared, sources of variability.

The observation, mentioned above, that WDC δ^{18}O and log(nssCa) are more coherent to finer timescales, than δ^{18}O and local accumulation is important. If dust emissions were the primary driver of the WDC nssCa record, this observation would lead to a surprising conclusion: that the processes driving dust emission in South America and those driving water-isotope distillation to West Antarctica are more connected than the processes driving water-isotope distillation to West Antarctica and those driving snow accumulation in West Antarctica. Such a conclusion seems inherently unlikely. The rainout model provides a simpler explanation for this apparent dissonance. The accumulation at WDC is dependent on moisture removal from the atmosphere at the latitude of WDC (ϕ_{WDC}), $-P(\phi_{WDC})$ in Equation 4, plus a variety of weather- and preservation-related noise. In the rainout model $-P(\phi)$ is determined by the saturated mixing ratio gradient at ϕ, though in reality is also influenced by weather-related noise. The δ^{18}O and log(nssCa) at WDC are also dependent on $-P(\phi_{WDC})$, but importantly both depend on the integration of $-P$ from their respective source latitudes through the mid- and high-latitudes, from ϕ_0 to ϕ_{WDC}. That integration, through overlapping latitudinal segments, reduces the influence of unshared noise on the resulting parameters. This naturally leads to the result that δ^{18}O, log(nssCa), and accumulation at the ice core site are all coherent at the longest timescales, but that δ^{18}O and log(nssCa) are more

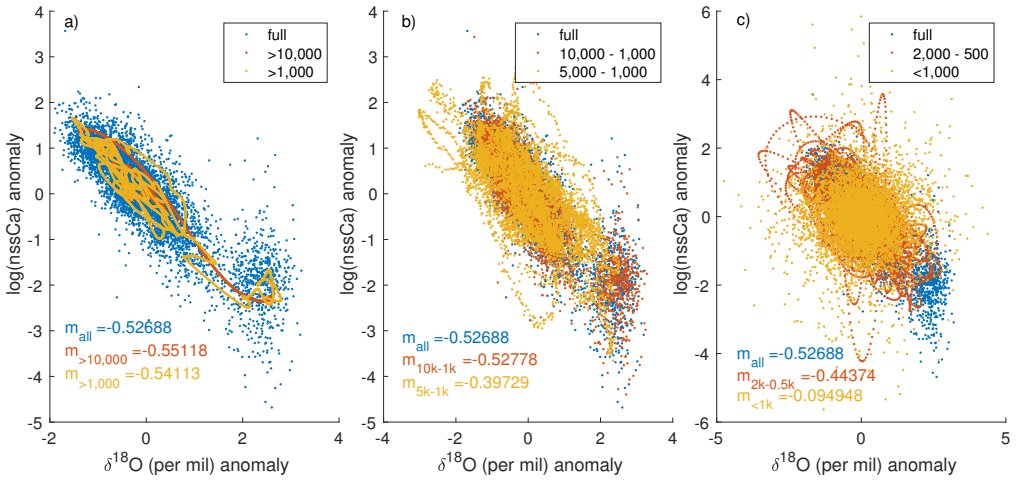

FIGURE S5. Comparison of WDC water isotope and aerosol records at different timescales of variability. All filtering was done with a fourth-order Butterworth filter. Data are presented as z-score anomalies. Slopes (m) of the linear fit between filtered δ^{18}O and log(nssCa) are shown in each panel. a) The full WDC δ^{18}P and log(nssCa) record (blue); low pass filtered records with periods >10,000 yr (red); and low pass filtered records with periods >1,000 yr (gold). b) Same as a) but for the full records (blue); band pass filtered records with 10,000-1,000 yr periods (red); and 5,000-1,000 yr periods (gold). c) Same as a) but for the full records (blue); band pass filtered records with 2,000-500 yr periods (red); and high pass filtered records with <1,000 yr periods (gold).

coherent at shorter timescales since the influence of noise is damped by the shared integration.

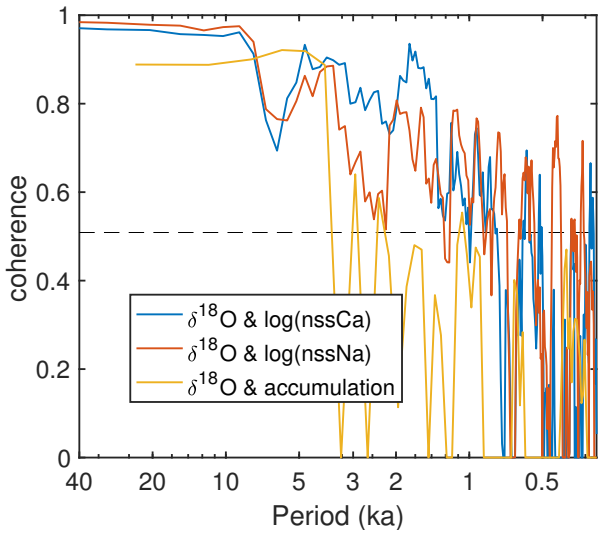

FIGURE S6. Multitaper spectral coherence of WDC δ^{18}O and log(nssCa) (blue), δ^{18}O and log(ssNa) (red), and δ^{18}O and local accumulation (gold)[20]. Coherence above the dashed black line is significantly coherent at the 95% confidence limit.

S3. AEROSOL VARIABILITY ACROSS MULTIPLE GLACIAL CYCLES

The negative-exponential relationship between aerosols and water isotopes is consistent across the vast majority of the domain in the WDC record including the glacial period and deglaciation (Figure S7). As noted in the main text, however, the slope of the relationship changes, specifically flattens, at interglacial δ^{18}O values, though this is a small fraction of the total range in the WDC records. Of interest is whether this is a persistent feature of interglacial periods and whether it suggests a change in the nature of the rainout process or the influence of other sources of aerosol variability.

This change in slope in the Holocene appears to be consistent across Antarctica and is seen in the EDC and EDML nssCa flux records[21] covering the same interval (Figure S3), as well as the Vostok dust[22], Siple Dome calcium[23], and Talos Dome iron records[24]. The East Antarctic ssNa records[21] show a change in slope of the negative-exponential relationship of the opposite sign, that is flattening at the coldest δ^{18}O values, rather than at the warmest.

As shown above (Figure S4), these types of changes in the slope are consistent with patterns of polar amplification influencing the rainout process, which cause contrasting slope changes between dust and sea salts within the same climate and different expression between sites. Changes in the scavenging efficiency with climate could also lead to changes in the slope of the aerosol water-isotope relationship. While plausible, we have no *a priori* expectation for changes in scavenging efficiency, though the required change would not be particularly large given the uncertainty in the parameter even in the modern

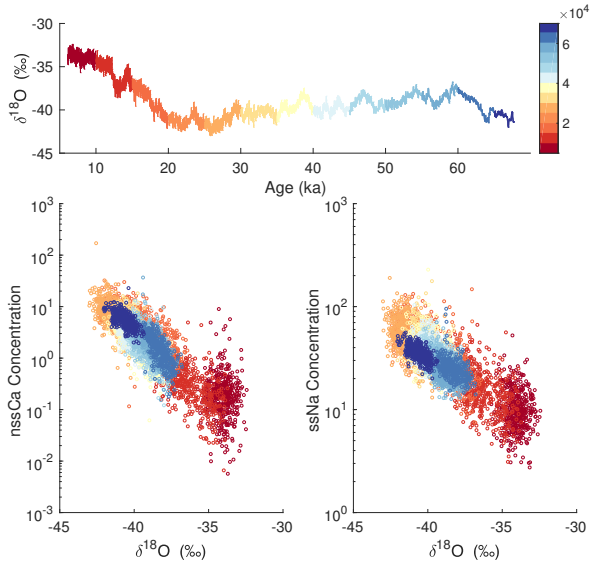

FIGURE S7. Water isotope and aerosol records from WDC. Top: WDC δ^{18}O colored by age interval. Bottom left and bottom right: nssCa vs δ^{18}O and ssNa vs δ^{18}O, respectively, both colored by age interval (in yrs binned by 5000 yr blocks).

climate (see Table S1). Other sources of aerosol variability, such as changes in source latitude or strength, could also change the slope of the relationship.

To assess the consistency of this relationship across multiple glacial cycles and the potential role of other sources of variability, we examine the 800 thousand year dust concentration record from EDC[25] (Figure S8a). We calculate the mean and median of the distribution of dust concentration for binned δD values (Figure S8b). Over multiple warm periods, the relationship shows a clear change in slope, though continues to be negative and exponential even at the highest δ values (Figure S8c).

At high accumulation sites like WDC, changes in the aerosol concentration in ice well-reflect those of the concentration in precipitation and air. At low accumulation sites like EDC, where dry deposition is a significant fraction of the total aerosol accumulation, the concentration in ice is affected by the dry-deposition and snow-accumulation rates, as well as the concentration in precipitation and air. Using the simple model, we calculate the aerosol concentration in ice for the EDC site to directly compare to the dust concentration as measured. The concentration in ice is

$$C_{ice} = \frac{C_{air} v_{dry}}{a \rho_{water}} + C_{precip} \tag{S2}$$

where v_{dry} is the dry deposition rate (about 0.1 to 0.3 cm s^{-1} for high latitude icesheets[2]) and a is the snow accumulation rate (about 3 cm yr^{-1} at the modern EDC site[25]), which

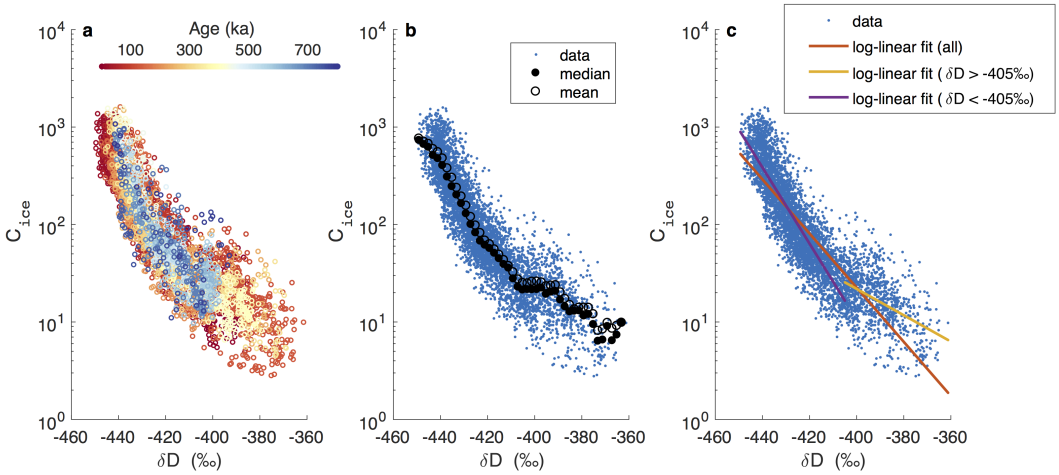

FIGURE S8. Measured relationship between dust concentration in ice and δD at EDC for 800 ka. **a)** Dust concentration in ice (C_{ice}, $\mu g/kg$) versus δD at EDC[25;26], colored by the age of the sample. **b)** Measured relationship (blue dots) and mean (black, open circles) and median (black, filled circles) C_{ice} for binned δD values. **c)** Fitted log-linear relationships for all data (red), the data when δD $>$ -405‰ (yellow), and the data when δD $<$ -405‰ (purple).

we assume is proportional to removal of atmospheric moisture at the grid point in the model and which changes with climate.

The changes in slope in the EDC dust water-isotope relationship are consistent with a poleward migration of aerosol source latitude during interglacials and/or an *increase* in the aerosol-source strength during interglacials (the opposite sign of the prevailing paradigm for source strength changes). To demonstrate this we run the rainout model through a range of climate states to reproduce the water-isotope variability at the EDC site.

We consider a climate-state dependent change in mean dust-source latitude (ϕ_0), (Figure S9a-b), as well as an idealized change in dust-source strength (C_0) that increases during warmer climates (Figure S9c-d). We find that a modest change of 1.5° in dust-source latitude agrees well with the change in slope in the data, as would a 3-fold increase in dust-source strength. Finally, concurrent changes in rainout, dust-source latitude, and source strength can together influence the slope of the dust water-isotope relationship (Figure S9e-f), and can readily explain the complexity in the observed slope changes.

These idealized patterns are not meant to be reconstructions of ϕ_0 or C_0 in the past, but simply demonstrations of their effect on the dust water-isotope relationship. We note that even in these cases, the rainout effect dominates the aerosol variability. These other sources appear to reduce variability that might be otherwise expected, merely changing the slope of the relationship with water isotopes.

The average of mid-latitude records for the most recent glacial-interglacial transition (Figure 4) suggest a decrease, rather than increase, of dust emission strength during the warm period, the opposite sign of the idealized changes imposed in Figure S9. While a 3-fold increase during interglacials is narrowly within the spread of some lower-latitude estimates for the Holocene, it is not of those from marine records corrected for sediment redistribution[27]. The marine and ice-core records together with our modeling may suggest that a poleward shift in dust source latitude is the more likely source for these changes than an increase in total dust emission. The log-normal scatter around the negative-exponential relationship increases slightly during the warm periods, coincident with the change in slope. This too is consistent with a poleward migration of the dust-source latitude. A poleward shift of the distribution of dust emission is consistent with a relative increase in emission form higher-latitude sources, which would be those most important to Antarctica (Figure S2). Such a poleward shift in source latitude and/or an increase in (higher-latitude) dust-source strength may be consistent with the interglacial retreat of South American glaciers.

These observations and modeling are not sufficient on their own to uniquely identify either a change in source strength or latitude, though such conclusions may be possible with more comprehensive analysis. This does, however, highlight the value of our approach. The rainout process provides a well-justified model of the system, from which deviations should be used to identify intervals of interest and quantify the influence of other sources of variability.

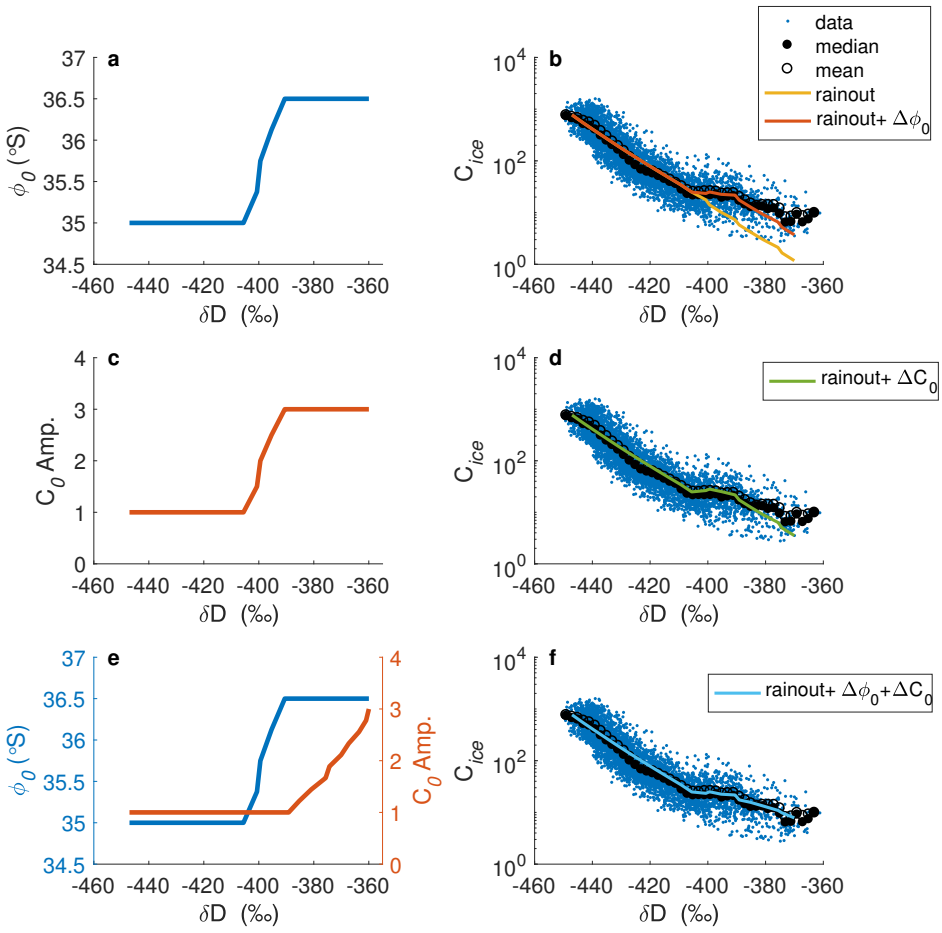

FIGURE S9. Observed and modeled relationship between dust concentration in ice and δD for EDC across multiple glacial cycles. **a)** An idealized change in mean dust source latitude (ϕ_0) with climate (represented by δD at the EDC site). **b)** Measured concentration of dust (C_{ice}, $\mu g/kg$) and δD of ice at EDC[25;26] (blue dots). Mean (black, open circles) and median (black, filled circles) C_{ice} for binned δD values. Modeled relationship between C_{ice} and δD at EDC due to the rainout process (yellow) and the rainout process plus the change in ϕ_0 shown in panel a (red). $\omega_{dust} = 1700$ for results shown here. **c)** An idealized pattern of changing dust source strength amplification (C_0 Amp.) with changing climate. **d)** Same as panel b) but for the modeled relationship (green) due to the rainout process and the changing C_0 shown in panel c). **e)** Idealized change in ϕ_0 and C_0 Amp. that increases during the warmest climate. **f)** Same as panel b) but for the modeled relationship (light blue) due to the rainout process and the idealized changes in ϕ_0 and C_0 shown in panel e.

S4. Aerosols and rainout in comprehensive models

Aerosols such as dust and sea salts are simulated in comprehensive climate models[28–30]. However comparisons of paleoclimate records and simulations of past changes in dust production and deposition have yielded mixed results. In general the simulations do not reproduce orders-of-magnitude changes in dust-source emissions[4;31–33]. Many models do reproduce 2-3 fold changes in low- to mid-latitude dust emissions during the LGM[4;31;32] in agreement with low-latitude proxy records[30]. Some models do not find significant changes in dust lifetime in the LGM compared to modern but also underestimate changes in Antarctic deposition of dust by orders of magnitude[31–33]. It has been been suggested that early global dust models lacked the necessary complexity in dust source region dynamics to reproduce the variability recorded in ice cores, but thorough investigations of many dust-production mechanisms are still unable to yield 10-100 fold changes in production[33]. There is recent indication that models may underestimate the efficiency of aerosol rainout and thus the changes in aerosol lifetime for a given change in precipitation. For example ref. [30] doubled dust solubility and below-cloud scavenging, which improved the spatial patterns of dust burden compared to modern observations and significantly increased simulated LGM changes in Antarctic dust deposition compared to previous studies[4;30].

We examine model results from the CESM Large Ensemble Experiment[5], run under different sets of boundary conditions. We examine mean fields from 100 years of an 1850 control run and the means of the first 94 years of an RCP8.5 forcing scenario. The nature of the change in boundary conditions isn't important in this test; we are simply interested in the changes in the hydrological cycle and aerosols for a given change in mean state. In Figure S10 we show that changes in mean temperature lead to changes in integrated precipitation that increase toward the poles. These changes in integrated precipitation are in turn associated with exponential changes in high-latitude aerosols, both dust and sea salts, between their sources and deposition sites, in agreement with the results of our model. The change in aerosols are shown as amplification from their initial source strength, identified as the peak aerosol burden in the zonal mean (about 35°S for dust and 60°S for sea salts in this model). Changes in sea salts are muted compared to those of dust, just as in our model. It is interesting that the source-emission strengths of both aerosols are actually increased in the warmer mean state (the RCP 8.5 scenario) compared to the colder mean state (the 1850 scenario). However, changes in the hydrologic cycle are strong enough to overwhelm this source-emission effect for both aerosols: despite increases in source emission, absolute aerosol burdens over Antarctica in the warm scenario are less than the cold scenario. This analysis demonstrates that the underlying physics of the rainout model, while a simplification of more complex dynamics, are robust. Changes in the hydrologic cycle and rainout dominate changes in high-latitude aerosols.

While the GCM displays poleward changes in aerosols as predicted by the rainout model, the magnitude of the poleward depletion is less than in the simple rainout model when run with the zonal mean temperature profiles from the 1850 and RCP 8.5 scenarios.

There may be several sources for this discrepancy including the rudimentary estimation of precipitation and aerosol rainout in the simple model. However, there is a strong indication that CESM actually underestimates the strength of the scavenging process in these control runs. As seen in Figure S10, dust burden decays by about 1.5 orders of magnitude from the midlatitudes to the pole in the control run. Modern observations however suggest this decay should be on the scale of 3-4 orders of magnitude[4;30]. If the model is underestimating the current strength of the rainout process, that is the amount of aerosol removed for a given amount of precipitation, it will also underestimate the changes in aerosols driven by the rainout process, perhaps by orders of magnitude. As noted above, ref.[30] find that by significantly increasing the strength of scavenging in CAM (the atmosphere component of CESM) they are better able to match modern observations and past changes.

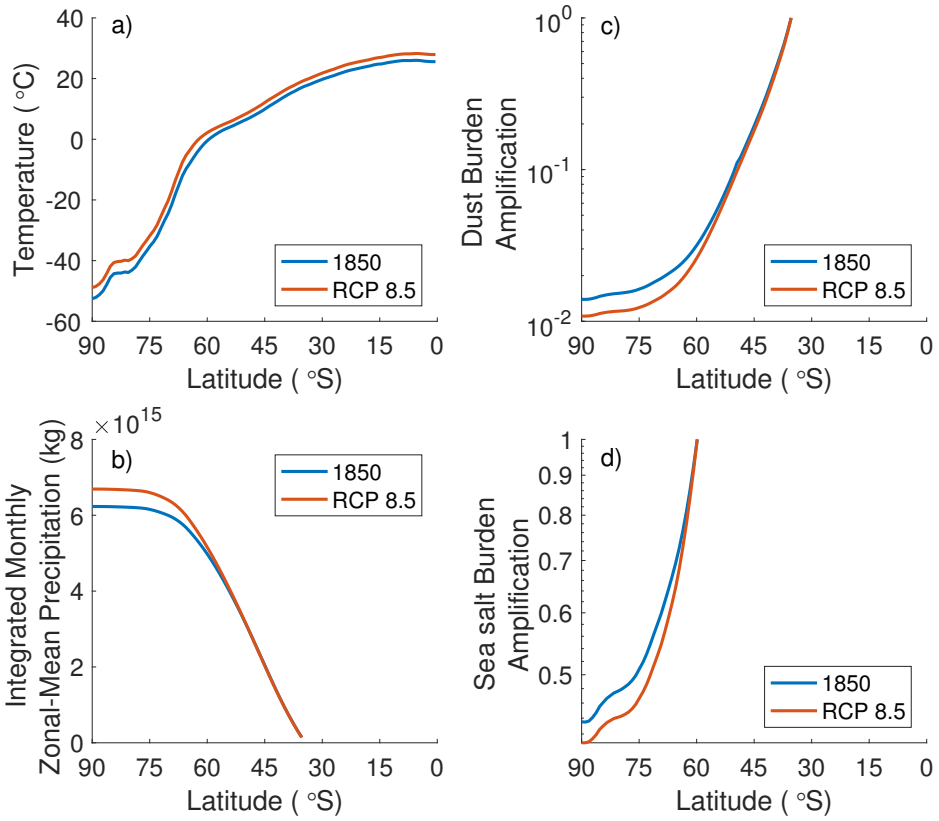

FIGURE S10. a) Zonal mean, century mean Southern Hemisphere surface temperature for the 1850 (blue) and RCP 8.5 (red) scenarios. b) Integrated monthly precipitation between 35°S and the pole for both scenarios. c) Dust aerosol burden (kg m^{-2}) as a fraction of source strength for both scenarios. sea-salt aerosol burden (kg m^{-2}) as a fraction of source strength for both scenarios.

S5. IMPLICATIONS FOR AEROSOL INFLUENCE ON PAST RADIATIVE FORCING

Aerosols affect the radiation budget of the climate system both directly through scattering and absorption and indirectly through interaction with clouds[34]. The aerosol optical depth quantifies the extinction of incoming solar radiation by dust in the atmosphere and scales with the atmospheric dust burden. Uncertainty in the magnitude of dust aerosol forcing in the past is one of the largest sources of uncertainty in estimating climate sensitivity from paleoclimate data[35]. Spatial heterogeneity in that forcing is especially uncertain[36].

The interpretation of the cause of aerosol variability in ice cores has important implications for the magnitude and spatial pattern of past changes in the atmospheric dust

burden, optical depth, and radiative forcing. If dust-emission strength is the primary driver of ice-core aerosol variability, this implies order-of-magnitude changes in the aerosol optical depth everywhere between the midlatitude source and the high latitudes. If, on the other hand, the rainout process is the dominant driver of ice-core variability, there may have been order-of-magnitude changes at the poles, but comparatively little change at mid- and low-latitude sources. This has important implications for changes in the magnitude and variability of past radiative forcing and its spatial pattern, which in turn has implications for climate sensitivity and feedbacks.

Here we examine the zonal-mean dust burden and the 500 nm aerosol optical depth from the 100 year preindustrial experiment from the CESM Large Ensemble[5], shown in Figure S11a. The two variables are well correlated, particularly in the mid- and high-latitudes of the Northern Hemisphere (NH) and Southern Hemisphere (SH), Figure S11b, reflecting the well-known link between dust aerosols and radiative forcing[34]. In Figure S11c and d, we show schematics of possible past spatial patterns of Southern Hemisphere aerosol optical depth, based on the correlation of aerosol optical depth to aerosol burden in the model. In red, we show the preindustrial pattern from the CESM Large Ensemble. In light blue, we show the same pattern but multiplied by an order of magnitude across all latitudes, a pattern that might be expected if ice-core variability primarily reflects source-emission changes (LGM_{source}). In contrast, we also show a schematic pattern that might be expected if ice-core records predominantly reflect variability in the rainout process as described in this study ($LGM_{rainout}$, dark blue).

Studies which take ice-core aerosol records to reflect the temporal variability of *global* aerosol radiative forcing (e.g. ref[35;36]) overestimate changes in radiative forcing between the glacial and interglacial and may miss important changes in the spatial pattern of that forcing. Studies ignoring changes in aerosol radiative forcing (e.g. ref[11]) likely underestimate changes in the global mean forcing and spatial pattern. In the Paleoclimate Model Intercomparison Project, for example, models either compute aerosols on-line or use the preindustrial aerosol loading[37], for past climate scenarios. The preindustrial pattern likely underestimates changes in forcing in the middle and high latitudes. The extent to which models with on-line aerosols underestimate the rainout effect[30] may bias the simulated spatial pattern of aerosol loading and associated radiative forcing. The paleoclimate data support a spatial pattern of aerosol optical depth during the LGM that had modest and potentially variable amplification at the middle and low latitudes, but exponential amplification of aerosol optical depth toward the poles (Figure 4 and Figure S12).

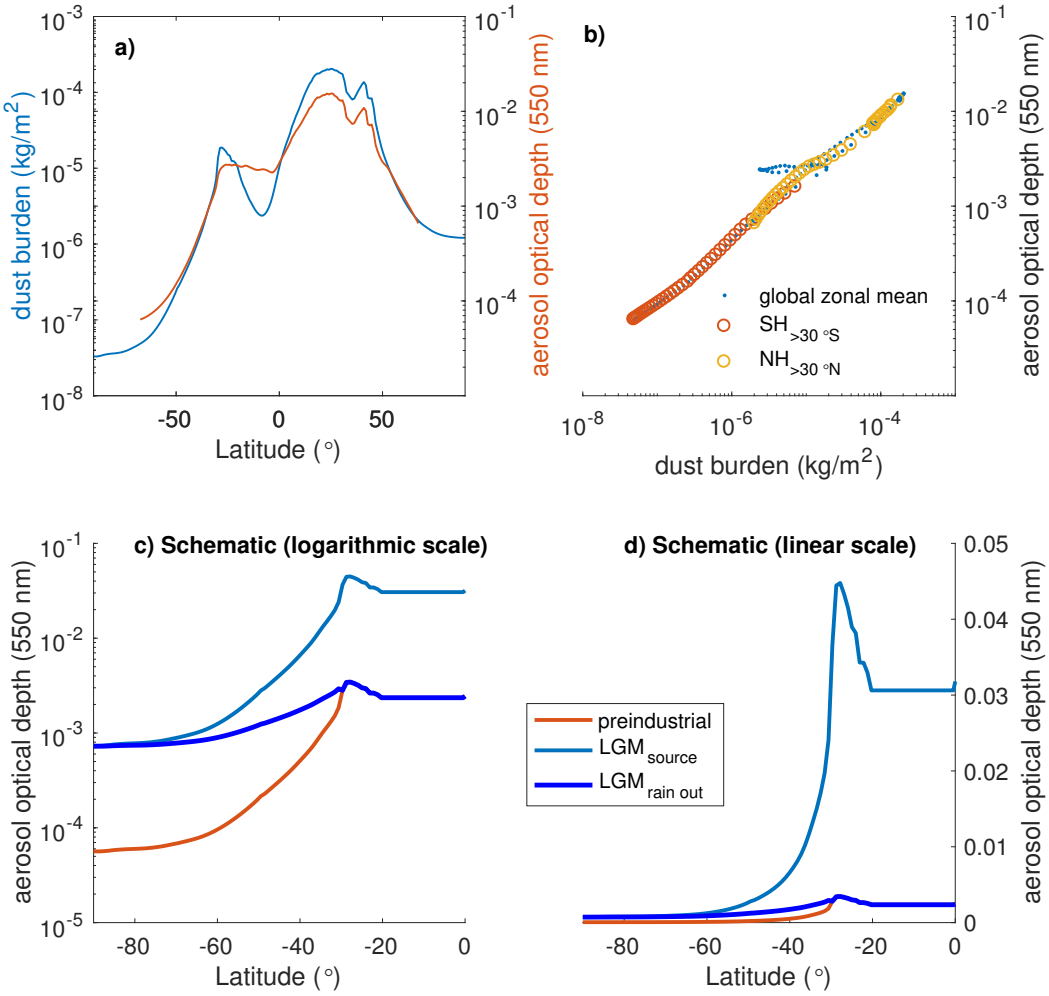

FIGURE S11. a) and b) Comparison of the zonal mean dust burden and the 500nm aerosol optical depth from the 100 year preindustrial experiment from the CESM Large Ensemble. c) and d) Schematic of aerosol optical depth for the preindustrial (red), and two hypothetical LGM-like scenarios: one in which preindustrial dust burdens are amplified by an order of magnitude at all latitudes (LGM_{source}, light blue), in line with large dust-emission changes; and another in which dust burdens show no change at the source but are amplified toward the pole due to changes in the rainout process ($LGM_{rainout}$, dark blue).

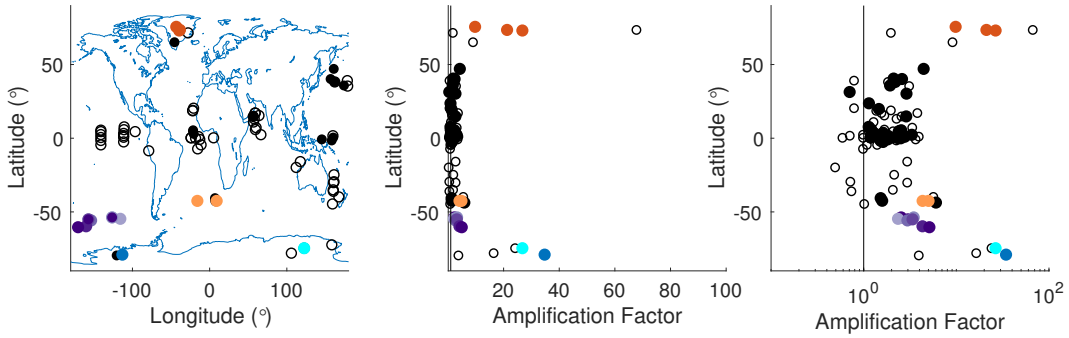

FIGURE S12. a) Global map of dust records as described in the main text and Figure 4, colored consistently. Dust amplification against latitude for all records shown in panel (a) on a linear scale (b) and log scale (c). Vertical black line in b) and c) at amplification of 1 (i.e. no change).

S6. Compilation of Mass Scavenging Efficiencies

The mass-scavenging ratio, ω, quantifies the efficiency of wet removal, with units $\frac{\text{g aerosol}}{\text{g precipitation}} \div \frac{\text{g aerosol}}{\text{g air}}$. Measured empirically, this ratio is influenced by both in-cloud and below-cloud processes. We here compile measurements of the mass-scavenging ratio for calcium and sodium from several previous compilations[2;38–40], and the references therein. The summary statistics for calcium and sodium are presented in Table S1. The measurements compiled in Table S1 are predominantly from Northern Hemisphere midlatitude and polar environments. There is considerable variance in the measured mass-scavenging ratios, likely reflecting both environmental variability and the difficulty of the measurements. For both calcium and sodium, the data indicate central values in the range of 1-2$\times 10^3$. Values within this range may be equally likely. As presented above, our results are robust to uncertainty of ω within this range.

Empirical Mass-Scavenging ratio, ω							
aerosol	n	minimum	maximum	mean	median	25$^{\text{th}}$ percentile	75$^{\text{th}}$ percentile
Calcium	14	320	3983	1528	1267	892	1815
Sodium	16	360	7106	1910	1002	523	2300

Table S1. Compilation of mass-scavenging ratios from refs[2;38;40]. Summary statistics for both calcium and sodium include the number of independent measurements, n; the minimum, maximum, mean and median of those measurements; as well as the 25$^{\text{th}}$ to 75$^{\text{th}}$ percentile bounds of those measurements.

References

[1] Davidson, C. *et al.* Seasonal variations in sulfate, nitrate and chloride in the greenland ice sheet: relation to atmospheric concentrations. *Atmospheric Environment (1967)* **23**, 2483–2493 (1989).

[2] Wolff, E. & Bales, R. Chemical exchange between the atmosphere and polar snow: proceedings of the NATO advanced research workshop" Processes of chemical exchange between the atmosphere and polar snow", held at Il Ciocco, Italy, March 19-23, 1995]. *NATO ASI series (Series 1, Global environmental change)* **43** (1996).

[3] Delmonte, B. *et al.* Aeolian dust in East Antarctica (EPICA-Dome C and Vostok): Provenance during glacial ages over the last 800 kyr. *Geophysical Research Letters* **35** (2008).

[4] Albani, S., Mahowald, N. M., Delmonte, B., Maggi, V. & Winckler, G. Comparing modeled and observed changes in mineral dust transport and deposition to Antarctica between the Last Glacial Maximum and current climates. *Climate dynamics* **38**, 1731–1755 (2012).

[5] Kay, J. *et al.* The Community Earth System Model (CESM) large ensemble project: A community resource for studying climate change in the presence of

internal climate variability. *Bulletin of the American Meteorological Society* **96**, 1333–1349 (2015).

[6] Kaufman, Y. J., Tanré, D. & Boucher, O. A satellite view of aerosols in the climate system. *Nature* **419**, 215–223 (2002).

[7] Rankin, A., Auld, V. & Wolff, E. Frost flowers as a source of fractionated sea salt aerosol in the polar regions. *Geophysical Research Letters* **27**, 3469–3472 (2000).

[8] Sugden, D. E., McCulloch, R. D., Bory, A. J. M. & Hein, A. S. Influence of Patagonian glaciers on Antarctic dust deposition during the last glacial period. *Nature Geoscience* **2**, 281–285 (2009).

[9] Gili, S. *et al.* Provenance of dust to antarctica: A lead isotopic perspective. *Geophysical Research Letters* **43**, 2291–2298 (2016).

[10] Ginoux, P., Prospero, J. M., Gill, T. E., Hsu, N. C. & Zhao, M. Global-scale attribution of anthropogenic and natural dust sources and their emission rates based on modis deep blue aerosol products. *Reviews of Geophysics* **50** (2012).

[11] Otto-Bliesner, B. L. *et al.* Last glacial maximum and Holocene climate in CCSM3. *Journal of Climate* **19**, 2526–2544 (2006).

[12] Masson-Delmotte, V. *et al.* Past and future polar amplification of climate change: climate model intercomparisons and ice-core constraints. *Climate Dynamics* **26**, 513–529 (2006).

[13] Cuffey, K. M. *et al.* Deglacial temperature history of West Antarctica. *Proceedings of the National Academy of Sciences* **113**, 14249–14254 (2016).

[14] Markle, B. R. *Climate dynamics revealed in ice cores: advances in techniques, theory, and interpretation*. Ph.D. thesis, University of Washington (2017).

[15] Markle, B. R. *et al.* Global atmospheric teleconnections during Dansgaard-Oeschger events. *Nature Geoscience* **10**, 36–40 (2017).

[16] Schoenemann, S. W., Steig, E. J., Ding, Q., Markle, B. R. & Schauer, A. J. Triple water-isotopologue record from WAIS Divide, Antarctica: Controls on glacial-interglacial changes in 17Oexcess of precipitation. *Journal of Geophysical Research: Atmospheres* **119**, 8741–8763 (2014).

[17] Fischer, H., Siggaard-Andersen, M.-L., Ruth, U., Röthlisberger, R. & Wolff, E. Glacial/interglacial changes in mineral dust and sea-salt records in polar ice cores: Sources, transport, and deposition. *Reviews of Geophysics* **45** (2007).

[18] Hwang, Y.-T. & Frierson, D. M. W. Increasing atmospheric poleward energy transport with global warming. *Geophysical Research Letters* **37**, n/a–n/a (2010).

[19] Roe, G. H., Feldl, N., Armour, K. C., Hwang, Y.-T. & Frierson, D. M. The remote impacts of climate feedbacks on regional climate predictability. *Nature Geoscience* **8**, 135–139 (2015).

[20] Fudge, T. *et al.* Variable relationship between accumulation and temperature in West Antarctica for the past 31,000 years. *Geophysical Research Letters* **43**, 3795–3803 (2016).

[21] Fischer, H. *et al.* Reconstruction of millennial changes in dust emission, transport and regional sea ice coverage using the deep EPICA ice cores from the Atlantic

and Indian Ocean sector of Antarctica. *Earth and Planetary Science Letters* **260**, 340–354 (2007).

[22] Petit, J.-R. *et al.* Palaeoclimatological and chronological implications of the vostok core dust record. *Nature* **343**, 56 (1990).

[23] Kreutz, K. & Koffman, B. *ICE CORE METHODS| Glaciochemistry* (Elsevier, 2013).

[24] Vallelonga, P. *et al.* Iron fluxes to Talos Dome, Antarctica, over the past 200 kyr. *Climate of the Past* **9**, 597–604 (2013).

[25] Lambert, F. *et al.* Dust-climate couplings over the past 800,000 years from the EPICA Dome C ice core. *Nature* **452**, 616–619 (2008).

[26] Jouzel, J. *et al.* Orbital and millennial antarctic climate variability over the past 800,000 years. *science* **317**, 793–796 (2007).

[27] Kienast, S., Winckler, G., Lippold, J., Albani, S. & Mahowald, N. Tracing dust input to the global ocean using thorium isotopes in marine sediments: Thoromap. *Global Biogeochemical Cycles* **30**, 1526–1541 (2016).

[28] Zender, C. S., Bian, H. & Newman, D. Mineral Dust Entrainment and Deposition (DEAD) model: Description and 1990s dust climatology. *Journal of Geophysical Research: Atmospheres* **108** (2003).

[29] Li, F., Ginoux, P. & Ramaswamy, V. Distribution, transport, and deposition of mineral dust in the Southern Ocean and Antarctica: Contribution of major sources. *Journal of Geophysical Research: Atmospheres* **113** (2008).

[30] Albani, S. *et al.* Improved dust representation in the Community Atmosphere Model. *Journal of Advances in Modeling Earth Systems* **6**, 541–570 (2014).

[31] Mahowald, N. M. *et al.* Change in atmospheric mineral aerosols in response to climate: Last glacial period, preindustrial, modern, and doubled carbon dioxide climates. *Journal of Geophysical Research: Atmospheres* **111** (2006).

[32] Bauer, E. & Ganopolski, A. Aeolian dust modeling over the past four glacial cycles with CLIMBER-2. *Global and Planetary Change* **74**, 49–60 (2010).

[33] Li, F. *et al.* Toward understanding the dust deposition in Antarctica during the Last Glacial Maximum: sensitivity studies on plausible causes. *Journal of Geophysical Research: Atmospheres* **115** (2010).

[34] Stier, P., Seinfeld, J. H., Kinne, S. & Boucher, O. Aerosol absorption and radiative forcing. *Atmospheric Chemistry and Physics* **7**, 5237–5261 (2007).

[35] Friedrich, T., Timmermann, A., Tigchelaar, M., Timm, O. E. & Ganopolski, A. Nonlinear climate sensitivity and its implications for future greenhouse warming. *Science Advances* **2**, e1501923 (2016).

[36] Köhler, P. *et al.* What caused Earth's temperature variations during the last 800,000 years? Data-based evidence on radiative forcing and constraints on climate sensitivity. *Quaternary Science Reviews* **29**, 129–145 (2010).

[37] Schmidt, G. A. *et al.* Climate forcing reconstructions for use in PMIP simulations of the last millennium (v1. 0). *Geoscientific Model Development* **4**, pp33–45 (2011).

[38] Jaffrezo, J.-L. & Colin, J.-L. Rain-aerosol coupling in urban area: scavenging ratio measurement and identification of some transfer processes. *Atmospheric Environment (1967)* **22**, 929–935 (1988).

[39] Tegen, I. & Fung, I. Modeling of mineral dust in the atmosphere: Sources, transport, and optical thickness. *Journal of Geophysical Research: Atmospheres* **99**, 22897–22914 (1994).

[40] He, J. & Balasubramanian, R. Rain-aerosol coupling in the tropical atmosphere of southeast asia: distribution and scavenging ratios of major ionic species. *Journal of atmospheric chemistry* **60**, 205–220 (2008).